MODEL PREDICTIVE CONTROL DESIGN FOR THE SECONDARY FREQUENCY CONTROL OF MICROGRID CONSIDERING TIME DELAY ATTACKS

by

Zhengrong Chen

A Thesis Submitted in

Partial Fulfillment of the

Requirements for the Degree of

Master of Science

in Engineering

at

The University of Wisconsin-Milwaukee

May 2019

ABSTRACT

MODIFIED MODEL PREDICTIVE CONTROL STRATEGY FOR MICROGRID SECONDARY FREQUENCY CONTROL WITH TIME DELAY ATTACKS

by

Zhengrong Chen

The University of Wisconsin-Milwaukee, 2019
Under the Supervision of Professor Lingfeng Wang

Fast depleting fossil fuels and growing awareness of environmental protection have raised worldwide concerns, aiming to build a sustainable and smart energy ecosystem. Renewable energy generation plays an important role in providing clean power supply. However, the integration of a bulk renewable generation system would also introduce new forms of disturbances and uncertainties to impact the power quality, threatening the secure operation of the distribution network. Microgrid, as an emerging technology, is quite appealing to be interfaced with distribution systems due to its potential economic, environmental, and technical benefits. The microgrid differs from the “smart grid” with different control strategies to accomplish the goal of helping the power grid with load balancing and voltage control and assisting power markets. A hierarchical control structure for the microgrid is commonly designed to address all above issues both in islanded mode and grid-connected mode.

On the other hand, concerns about cybersecurity threats in the microgrid are steadily

rising, and enormous number of economic losses would occur if defense strategies are not stipulated and carried out. In the modern power system, distributed control system, intelligent measuring devices and Internet of Things (IoT) are highly recommended in microgrid systems, which lead to the vulnerability of communication channels. Cyber threats such as false data injection (FDI) attacks, denial of service (DoS) attacks, and time-delay switch attacks (TDS) can be effortlessly implemented through information and communication centers, compromising the secure operation of power systems. By theoretically analyzing the AC microgrid simulation model, the MPC control strategies, and the modified MPC method based on GCC estimation will be studied in this thesis.

In the second chapter, this thesis summarizes the start-art-of microgrid control, introducing a hierarchical control structure: primary control, secondary control, and tertiary control. These control levels differ in their speed of response, the time frame in which they operate, and infrastructure requirements. We focus on the centralized secondary frequency control system, which compensates the frequency deviation caused by primary control—P/f method.

Then, in Chapter 3, the isolated AC MG frequency control system including WTG, DEG, PV panel and energy storage system with MPC controller is modeled. Three case studies are designed in MATLAB/Simulink to illustrate the advantages of the MPC method compared with the traditional PI controller.

In the next Chapter, since state estimation based on precise status feedback of the system components is essential for the MPC controller to calculate corresponding control signal, the status feedback attack to BESS and FESS is considered. Correspondingly, an online status

switching method is proposed to detect the original statuses of BESS and FESS, updating the state estimation function to obtain desirable performance of frequency regulation.

Last, considering the time delay attack hacked by the adversary in the sensor, a modified MPC method based on GCC estimation is proposed to detect and track time delay attacks online. The model of proposed method to regulate frequency deviation is built in MATLAB. There are three case studies in this part: a constant time-delay attack with 0.1 pu load increase; a time-varying delay attack with 0.1 pu load increase; and a time-varying delay attack with changing load disturbance. By analyzing results of three cases, the effectiveness of the modified MPC method is proved.

© Copyright by Zhengrong Chen, 2019

All Rights Reserved

TABLE OF CONTENTS

ABSTRACT ii

LIST OF FIGURES viii

LIST OF TABLES x

LIST OF ABBREVIATIONS xi

ACKNOWLEDGMENTS xii

Chapter 1 ： Introduction 1

1.1 MG: background and motivation 1

1.2 MG: cyber-attack risk 3

1.3 Research objectives 5

1.4 Thesis contribution 6

Chapter 2： MG control state-of-the-art 8

2.1 Hierarchical structure 8

2.2 Primary control 9

2.2.1 Inverter output control 10

2.2.2 Power sharing control 11

2.3 Secondary control 13

2.3.1 Centralized frequency control 13

2.3.2 Distributed frequency control 15

Chapter 3： MG frequency control: modelling 17

3.1 Configuration of an islanded microgrid 17

3.1.1 Modelling of frequency response 17

3.1.2 Characteristics of output power of WTG and PV 19

3.1.3 The transfer functions of various generation subsystems 20

3.1.4 Transfer functions of different energy storage systems 20

3.1.5 System frequency variation 21

3.2 Conventional PI controller 21

3.2.1 Frequency control model 21

3.2.2 WTG model and PV model 23

3.2.3 Simulation in Simulink 24

3.3 Model predictive control 27

3.3.1 Principle of MPC 27
3.3.2 MPC controller for MG frequency control 28
3.4 Case study 31
3.4.1 Case design 31
3.4.2 Simulation result and discussion 32
Chapter 4: MPC status feedback attack 38
4.1 Attack description 38
4.2 Online switching method 40
4.3 Case study 41
Chapter 5: Modified MPC controller under time-delay attack 44
5.1 Time delay attack 44
5.2 MPC controller under time-delay attack 46
5.2.1 Modelling 46
5.2.2 Case study with known time-delay signal 47
5.3 Modified MPC with online time-delay estimation 50
5.3.1 Methodology 50
5.3.2 Generalized cross correlation 51
5.3.3 Algorithm of controller design 52
Chapter 6: Case study 54
6.1 Modified MPC model simulation 54
6.1.1 Case 1: constant time-delay attack 54
6.1.2 Case 2: time-varying delay attack 56
6.1.3 Case 3: two steps load disturbance 57
6.2 Discussion 59
Chapter 7: Conclusion and future work 60
7.1 Conclusion 60
7.2 Future work 61
REFERENCES 63

LIST OF FIGURES

Figure 1.1 Attacks on control loop 4

Figure 2.1 Hierarchical control levels of microgrid 8

Figure 2.2 Current and voltage control loops 10

Figure 2.3 P-f droop curve 12

Figure 2.4 Q-V droop curve 12

Figure 2.5 Centralized secondary control system for frequency regulation 14

Figure 2.6 Distributed secondary control system for frequency regulation 16

Figure 3.1 Single-line diagram of the ac MG 18

Figure 3.2 Conventional PI Frequency response model for the ac MG system 22

Figure 3.3 Wind turbine output 23

Figure 3.4 Solar radiation Φ and PV output power 24

Figure 3.5 Simulink scheme-PI 25

Figure 3.6 (a) Multiple step load disturbances (b) MG frequency response 26

Figure 3.7 Frequency control following a step load disturbance of 0.1 pu 26

Figure 3.8 MPC framework 28

Figure 3.9 Simulink scheme-MPC 30

Figure 3.10 Case1 control system scheme 32

Figure 3.11 Frequency control following a step load disturbance of 0.1 p.u 33

Figure 3.12 Case2 control system scheme 34

Figure 3.13 Frequency control following a step load disturbance of 0.1 p.u 35

Figure 3.14 Case3 control system scheme 35

Figure 3.15 Case 3 frequency control following a step load disturbance of 0.1 p.u 36

Figure 3.16 Comparison for three cases 36

Figure 4.1 Scheme of MPC status feedback attack..... 39

Figure 4.2 Status feedback attack online detection block 40

Figure 4.3 Frequency response under status feedback attack 42

Figure 4.4 Frequency response with online switching method under status feedback attack 43

Figure 4.5 Online detection of statues of BESS and FESS..... 43

Figure 5.1 A simplified load frequency control system under time-delay attack 45

Figure 5.2 Dynamic model of MPC frequency control with delay attack..... 46

Figure 5.3 MPC control block diagram under attack..... 46

Figure 5.4 Frequency respond when τ =0.1s..... 48

Figure 5.5 Frequency respond when τ =0.2s..... 48

Figure 5.6 Frequency respond when τ =0.4s..... 48

Figure 5.7 Frequency respond when τ =0.6s..... 49

Figure 5.8 Block diagram of proposed control technique..... 50

Figure 6.1 GCC delay estimation in case1..... 55

Figure 6.2 Frequency response following a step load disturbance of 0.1 pu 55

Figure 6.3 (a) Frequency output of microgrid system in case 2 (b) time-varying delay estimation..... 56

Figure 6.4 Two steps load disturbance..... 57

Figure 6.5 GCC time delay estimation in case 3..... 58

Figure 6.6 Frequency response in case 3 58

LIST OF TABLES

TABLE I RATED POWER OF DG UNITS AND LOADS 18

TABLE II THE PARAMETERS VALUES OF THE AC MG SYSTEM 23

TABLE III CASE STUDY DESIGN 32

LIST OF ABBREVIATIONS

MG	Microgrid
MPC	Model predictive control
IoT	Internet of things
FDI	False data injection
DoS	Denial of service
TDS	Time-delay switch
GCC	Generalized cross correlation
WTG	Wind turbine generation
DEG	Diesel engine generation
PV	Photovoltaics
BESS	Battery energy storage system
FESS	Flywheel energy storage system
FC	Fuel cell
PI	Proportional–integral
RES	Renewable energy source
DER	Distributed Energy Resources
DGRs	Distributed generation resources
DG	Distributed generators
CHP	Combined heat and power
LV	Low voltage
MV	Medium voltage
DSM	Demand side management
PCC	Point of common coupling
ICT	Information & communication technology
PMU	Phasor measurement units
LFC	Load frequency control
LMIs	Linear matrix inequalities
RMSE	Root-mean-square error
VSIs	Voltage-Source Inverters
VSC	Voltage-Source Converter
PLL	Phase locked loop
SISO	Single-input single-output
MIMO	Multi-input multi-output
SCS	Secondary control system

ACKNOWLEDGMENTS

I cannot express enough thanks to my advisor, Prof. Lingfeng Wang, for his constructive guidance in the cutting-edge research on reliability and cybersecurity of power systems and also for his kindness and support in my daily life and study. Moreover, I would like to thank Dr. Zhaoxi Liu who helped me develop the model and case studies of this thesis.

Secondly, I would like to express my sincere gratitude to the committee members, Prof. Yi Hu and Prof. Zeyun Yu for their insightful and valuable comments.

I also want to give enormous thanks to my labmates in the Laboratory of Trustworthy Cyber-Physical Systems and Infrastructures for your help and support.

I am also grateful for the financial support for me to perform the research of this thesis. This work was supported in part by the National Science Foundation under Award ECCS1711617, in part by the Research Growth Initiative Program of University of Wisconsin-Milwaukee under Award 101X360, and in part by the National Science Foundation Industry/University Cooperative Research Center on Grid-connected Advanced Power Electronic Systems (GRAPES) under Award GR-18-06.

Finally, I am grateful for the continued support and encouragement from my parents, family, and friends throughout my graduate education.

Chapter 1：Introduction

1.1 MG: background and motivation

With the development of electrical industry, bulk power systems and reliable supply of energy are highly emphasized. Growing concerns for the primary energy structure and aging infrastructure of current electrical transmission and distribution networks are increasingly challenging security, reliability and quality of power supply. According to the International energy agency [1], energy demand is set to grow by more than 25% to 2040, requiring more than $2 trillion a year of investment in new energy supply. Thus, renewable energy sources (RESs) are mostly appealing one which can be used as alternative generation units in the modern power system to meet the need of efficient energy supply and low carbon economy. The increasing penetration of the RESs has many advantages, but also introduces new challenges as whether those sources can operate stable beside conventional generation units or not.

It is worth noting that the power systems have always been “smart”, especially at the transmission level. However, the distribution level need to be transformed from passive to active networks, especially in the sense that control is distributed and power flows are bidirectional. Power generation can be linked to the customers load, taking all kinds of information to get the best operation point to reduce the total cost in real time.

The microgrid concept is a quite appealing to address above problems, specifically in the field of integrating Distributed Energy Resources (DER) into power system, as well as

distributed energy-storage systems. It consists of Distributed generators (DG, e.g. diesel engines, Micro Turbines, PV, wind turbines and CHP), storage units, Renewable energy Resources and loads [2-4]. Commonly, the energy-storage systems include pumped storage, compressed air energy storage, batteries, ultra-capacitors, flywheels, plug-in hybrid electric vehicles, etc. From a grid point of view, microgrids can be viewed as control entities within the power system. From the customer's point of view, microgrids and traditional low-voltage distribution networks provide heat and power requirements [5].

The MGs are mostly placed in the low voltage (LV) and medium voltage (MV) distribution networks [6]. With numerous micro-sources connected at the distribution level, there are new challenges, such as system stability, power quality, and network operation that must be resolved applying the advanced control techniques at LV/MV levels rather than high voltage levels which is common in conventional power system control.

The difference between microgrid and smart grid mainly depends on their control structure. So proper and complicated control is required for microgrid through which we can facilitate the effective integration of DER and ensure the operation to be stable and economically efficient. The principal roles of the microgrid control structure are [2]:

- Voltage and frequency regulation for both operating modes and seamless transition between two modes
- Proper load sharing and DER coordination
- Power flow control between the microgrid and the main grid
- Schedule and dispatch of units under supply and demand uncertainty
- Optimizing the microgrid operating cost

- Design of appropriate DSM schemes to allow customers to react to the grid's need

Microgrid can operate in both grid-connected and islanded operating modes to avoid huge loss caused by external faults [7]. In the grid-connected mode, active and reactive power can be shared through point of common coupling (PCC) connected to the main grid. So in the steady state, the system state e.g. voltage and frequency are necessarily following the nominal values. But in the islanded mode, the control issue becomes more difficult and intricate because of dynamic fluctuation and loss of communication with nominal points. More detailed control structure and advance control algorithm are required for the islanded mode to achieve voltage, current and frequency regulation in the MG.

1.2 MG: cyber-attack risk

Microgrid takes advantages of advanced control strategies, cost-competitive technologies and information & communication technology (ICT). In order to achieve stable and efficient operation of power system and DER units locally controlled, it's necessary to expend cyber network inter-connectivity so that information may flow freely and correctly. But, in the meanwhile, the communication channel and controller in power system will become more vulnerable to cyber threats. A campaign of cyberattacks disabled safety systems at the Davis-Besse nuclear power plant in 2003 [8]. In 2004, the U.S. Department of Energy (DOE) estimated the cost of the blackout is approximately $6 billion on cybersecurity threats in computer-based systems [9]. This large-scale blackout was caused by a software failure in the IT system, which shows that a deliberate attack would be much more catastrophic. In 2010, the *Stuxnet* norm was discovered, which was designed to target proprietary (Siemens) SCADA systems in an Iranian power plant. In 2015, the Ukrainian power grid was attacked by the cyber

attackers, which was considered the first cyber-attack event causing power blackouts [11].

Cyber attacks mainly include DoS attacks, false data injection attacks (FDI), malware, time-delay attacks and virus attacks. A DoS attack is a resource-exhausting attach that makes the server or communication network cannot provide normal services by sending a lot of useless command [12]. FDI attacks exploit the sensor (e.g. phasor measurement units, PMU) measurements by injecting false information, maliciously destroying the system performance. An example of FDI attacks in smart grid can be found in [13]. Time delay attacks are somehow like Dos attacks, which exist in power systems and influence the signals to maintain former state instead of current state, specifically in the sensing and control loops. The impact of time delays on the power system was discussed in [14-16].

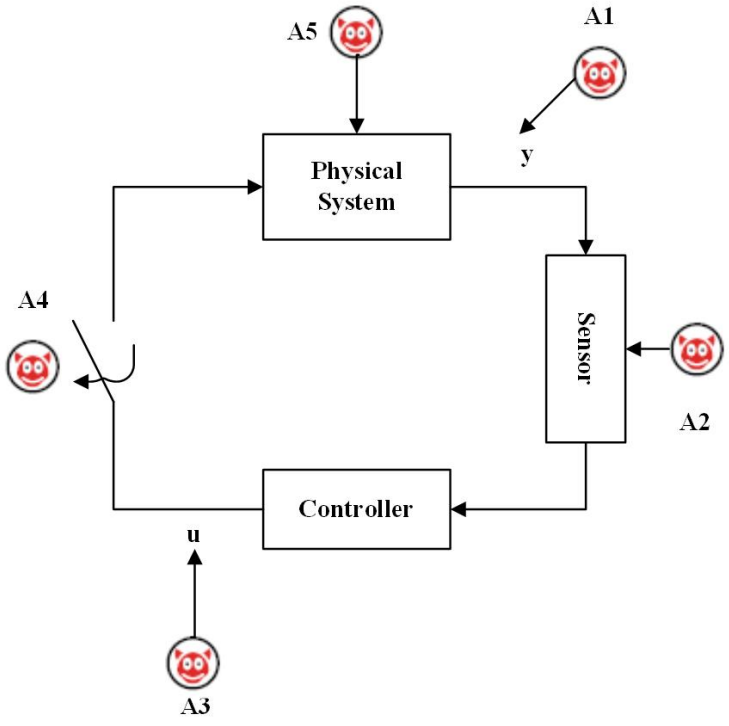

Figure 1.1 Attacks on control loop

From the view of control system, some attacks on control loop can be identified as Figure 1.1. A1 and A3 correspond to integrity attacks, where the adversary sends false information (e.g. an incorrect measurement, an incorrect time) from sensors or controllers. A2 and A4

correspond to DoS attacks and time-delay attacks. The adversary will prevent the controller from receiving correct sensor measurements or prevents actuators from receiving control commands. The attackers can launch a DoS attack or time-delay attacks by jamming communication channels, compromising devices and preventing them from sending data, attacking routing protocols, or flooding the network. Finally, A5 corresponds to a direct attack against actuators or an external physical attack on the plant [17].

Several studies have assessed the time delay attacks and their impact on the stability of power system. Reference [18] use phasor measurements with delays to design a two-level control structure, and small signal stability of the power system was considered. In [19], a delay-dependent robust method is proposed for analysis of a PID-type LFC scheme considering time delays. The time-delay estimator based on gradient descent method and a modified least mean square minimization technique was proposed in [20]. Authors in [22] take Lyaponuv-theory and linear matrix inequalities (LMIs) techniques to analyze the delay time bound of stable LFC scheme. However, there are few control methods that perform online estimation of dynamic time delays and real-time control of power systems. Furthermore, few studies considered the control of power systems with time delays introduced by adversary.

1.3 Research objectives

The control system is the key part of the microgrid with the goal to solve the power dispatch issue, decrease the loss of the transmission line and improve the reliability of electric power system. In the traditional microgrid control system, the close-loop controllers based on proportional-integral-derivative (PID) are widely utilized. However, due to the complex multi-objective regulation problems in modern MG systems and uncertainty caused by RES,

traditional PID controllers are unable to provide a proper performance. The MPC controllers can be much more powerful and flexible. Besides, MPC can effectively overcome the uncertainty and non-linearity of the process, and deal with the variables constraints in processing manipulated variables [22].

The present thesis focuses on the MG frequency regulation, as a secondary control issue. There are three following objectives:

1) Model the MG frequency control system in isolated mode

2) Apply MPC controller as a secondary control part

3) Consider the status feedback attack to FESS and BESS system

4) Prevent the impact of time-delay attack in the control system

1.4 Thesis contribution

This thesis work has been guided by the purpose to realize frequency control in MG and maintain a generation-load balance. Moreover, stability of MG frequency control system is evaluated when considering time-delay attack in the communication channel. Then, some adjustments must have to be applied to eliminate the instability and devastation caused by adversary.

The contribution in this thesis will be as following:

- Modeling the isolated ac MG system including WTG, DEG, PV panel and energy storage system.
- Realizing the MPC controller to control the frequency in the microgrid simulation in MATLAB/Simulink and comparing MPC method with the traditional PI controller to introduce its advantages.

- Creating an online switching method which takes RMSE to identify the real statuses of BESS and FESS when considering the status feedback attack to the state estimation of MPC controller.
- Proposing a modified MPC control algorithm based on a GCC time-delay estimation to obtain stable frequency regulation in real time, when considering constant or time-varying delay attack.

Chapter 2：MG control state-of-the-art

2.1 Hierarchical structure

With the regard to the principal roles of the microgrid control scheme, a hierarchical control structure is required to address different significances and time scales among microgrid control demand. Hierarchical control strategy consists of three levels, namely the primary, secondary, and tertiary controls, as shown in Figure 2.1. These control levels differ in their (i) speed of response and the time frame in which they operate, and (ii) infrastructure requirements (e.g., communication requirements) [22,23].

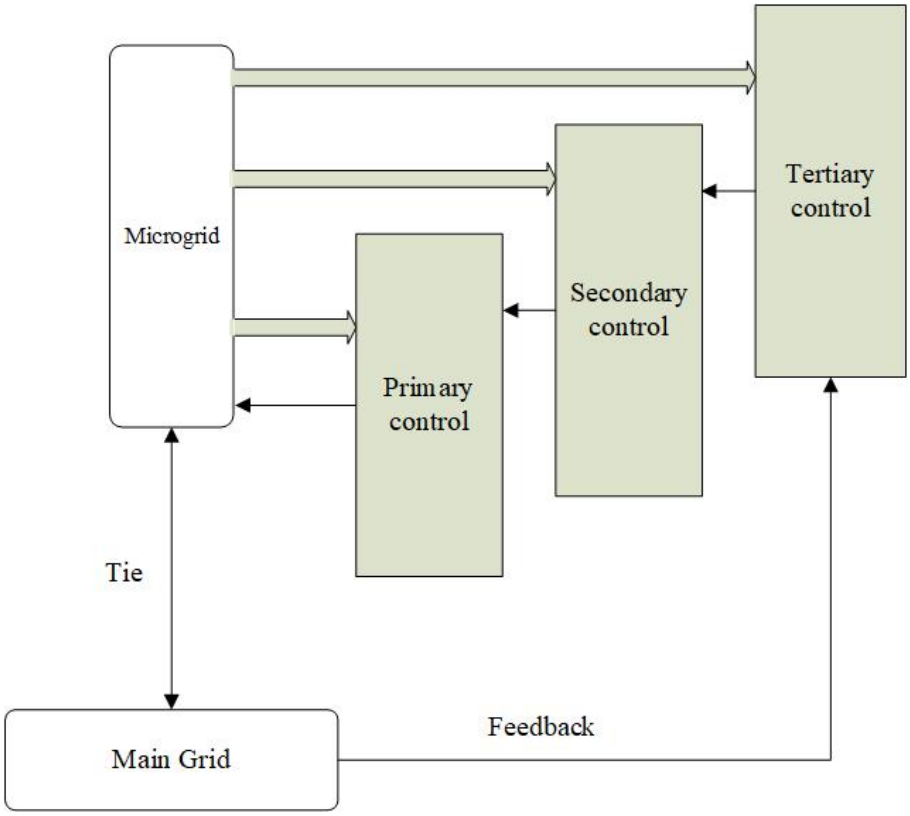

Figure 2.1 Hierarchical control levels of microgrid

The primary control, known as local control, maintains voltage and frequency stability of the microgrid. Based on local measurements, islanding detection, output control and power

sharing (and balance) control are included in this category. It is essential to provide independent active and reactive power sharing controls for the DERs in the presence of both linear and nonlinear loads. Thus, Voltage-Source Inverters (VSIs) are used as interface for DC sources. Meanwhile, inverter output controllers should control and regulate the output voltages and currents to satisfy power sharing control. The secondary control is responsible for the reliable, secure and economical operation of microgrids in either grid-connected or stand-alone mode, compensating for the voltage and frequency deviations caused by the operation of the primary controls. Ultimately, the tertiary control is the highest level of control and manages the optimal operation of all microgrids interacted. This control level provides signals to secondary level controls at microgrids and other subsystems that form the full grid. Tertiary control can be regarded as part of the host grid, and some parts beyond the microgrid. Therefore, this control level is not discussed in this thesis.

2.2 Primary control

The primary control is designed to address the following tasks:

- To stabilize voltage and frequency due to the mismatch between the power generated and consumed.
- To offer plug and play capability for DERs and properly share the active and reactive power among them.
- To regulate the currents to protect power electronic devices and the DC-link capacitor.

As more RES are commonly used in modern power system to improve energy structure, voltage-source inverters (VSIs) are required as interface for DC sources (e.g. solar power and wind power). VSI controllers are composed of two stages: inverter output controller and DG

power sharing controller.

2.2.1 Inverter output control

The inverter output control typically consists of an outer loop for voltage control, and an inner loop for current regulation. These inner control loops are commonly referred to as zero-level control, which have fast response speed and can keep the manipulated variables tracking the references [24].

The primary control will provide the reference points for the voltage and current control loops of DERs [25]. The nested voltage and frequency control loops are shown in Figure 2.2. The error signal, obtained by sensed signal from AC bus and reference signal, will be processed by voltage controller to compute the corresponding control signal. And inner current control loop, conventionally with additional feed-forward current compensation to regulate the current of VSC output.

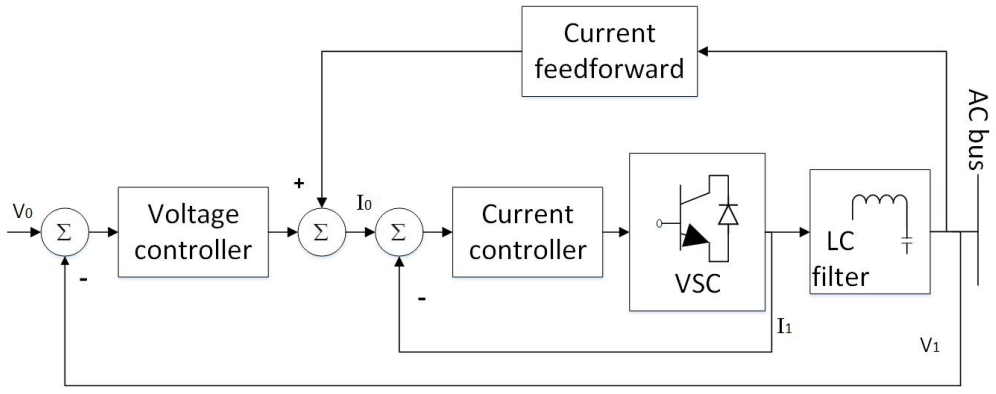

Figure 3.2 Current and voltage control loops

In general, PI controllers are commonly used in above control loops, obtaining content performance of voltage and current regulation. Besides, multivariable control methods have been proposed in [26], [27] to improve the dynamic response of microgrids and ensure robust

stability against uncertainties in load parameters due to presence of nonlinear loads.

2.2.2 Power sharing control

The usual method to accomplish active and reactive power sharing is to use Q-V and P-f droop control algorithms [22,23,28]. When two points in the network are operating at different frequencies there is an increase of active power delivery from the location of higher frequency to the location of lower frequency. As this happens, the two frequencies tend to drift towards a common average value until the new steady state is reached (self-synchronizing torque). If the network exists mismatch for reactive power, the situation can be solved by regulating voltage in the system.

When considering different configuration of converters, there are several methods to address active and reactive power control such as centralized [29], master-slave [30], decentralized [31] and droop [32]. Due to space limitation, this thesis mainly presents 2.2.3 Droop control method.

In droop control, the relationship between real power/frequency and reactive power/voltage can be expressed as [25]:

$$\begin{cases} \omega_0 = \omega^* - D_p P \\ V = V^* - D_Q Q \end{cases} \tag{2.1}$$

where V^* and ω^* are the DER output voltage RMS value and nominal frequency, respectively. The droop coefficients, D_p and D_Q, can be adjusted either heuristically or by tuning algorithms.

By linearizing it, frequency droop characteristic is

$$\Delta\omega_0 = \Delta\omega^* - D_p \Delta P \tag{2.2}$$

The droop characteristic curve is shown in Figure 2.3 and Figure 2.4.

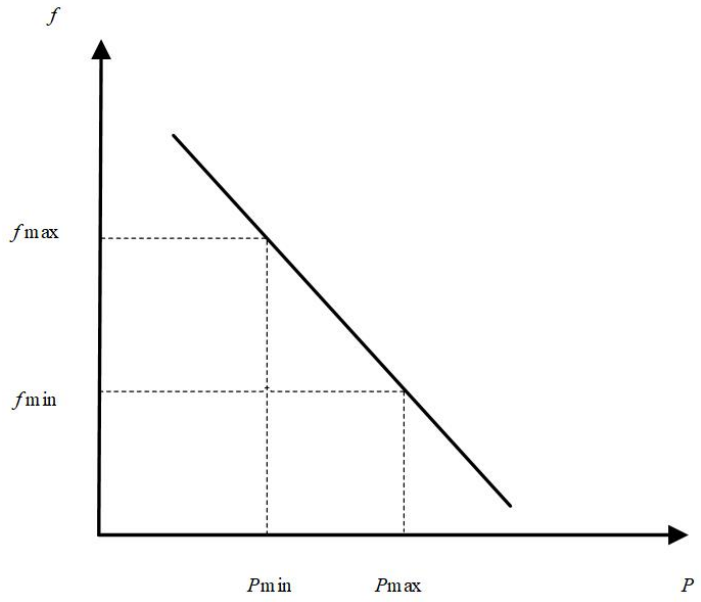

Figure 4.3 P-f droop curve

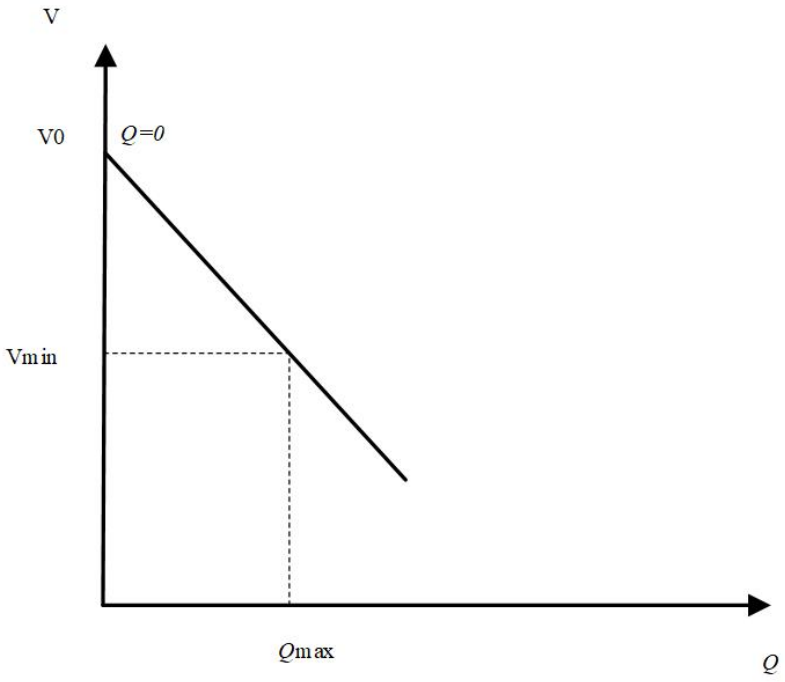

Figure 5.4 Q-V droop curve

The advantages of droop control are that it can be implemented with no communication links and the control action is merely based on local information. Those features make droop control more flexible and reliable than other methods. Some works address the scheduling of

the droop coefficients for frequency regulation in the MGs [33]. As described in [34], [35], frequency stability in a power system means preserving steady frequency following a heavy disturbance with minimum loss in loads and generation units.

However, in the steady state, the system will settle down to a new operating point where the MG frequency and voltage are not equal to the nominal value. Therefore, in some studies, a secondary control which compensate the voltage and frequency deviations caused by the droop control is required to be designed.

2.3 Secondary control

As mentioned, secondary control is responsible for the secure, economical and reliable operation of the microgrid. When in the steady state, secondary control will restore the microgrid voltage and frequency, compensating the deviations caused by the primary control. This control hierarchy will have slower dynamic response than that of the primary, which reduces the harmonic content of the voltage waveform.

There are two topologies for secondary control: centralized and distributed. While the centralized topology proposes a central controller to make decisions, the distributed topology allows the interaction of various units within the microgrid and realization of self-control. It's obvious that the distributed approach can exhibit the desirable plug-and-play feature, which may be the trend of microgrid control topology.

This thesis focuses on frequency regulation of the microgrid. A related detailed description of the centralized and decentralized approaches is presented next.

2.3.1 Centralized frequency control

The centralized secondary control scheme is depicted in Figure 2.5. In general terms, the frequency is usually estimated by a phase locked loop (PLL) and compared with the reference value ω_n. Then the secondary controller will compute a correcting signal ω_s sending to the primary controller through communication link. Finally, frequency regulation of the distributed generation resources (DGRs) can be archived by the function of centralized secondary controller. In addition, centralized secondary control system can operate using a unidirectional low bandwidth communication channel, which may show robustness in the dynamic situation. The reference value ω_n would be different for islanded mode and grid-connected mode. In the islanded operating mode, the reference value ω_n can be directedly set by desirable operating points. On the other hand, active power of main grid needs to be considered in the grid-connected operating mode, which is calculated by tertiary control.

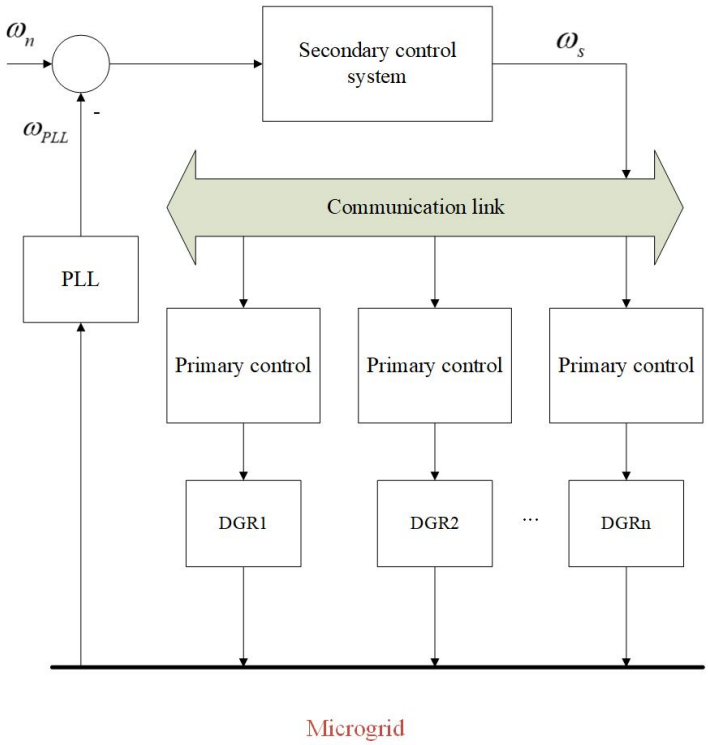

Figure 6.5 Centralized secondary control system for frequency regulation

According to reference [36], centralized controllers could be still considered more robust

and reliable than distributed one in MGs located in developing countries and/or rural areas where good communication infrastructure is not always available. However, huge losses may occur due to a system collapse if failure happens to the communication channel. Hence, it's essential to discuss the security and stability of MG secondary control.

2.3.2 Distributed frequency control

The distributed control framework, in comparison of the centralized control strategy, uses the recent advances in communication technologies, such as WiFi and Zigbee technologies, and also new algorithms for exchange of information (such as gossip, consensus, OpenFMB) [37]. A typical distributed secondary control is shown as Figure 2.6. In this case, each generation unit is provided with secondary control capacity to correct the frequency deviation. Moreover, each DGR is equipped with PLLs to estimate voltage and frequency at PCC. In some area, the distributed secondary control system looks promising because of its autonomous capacity for each DGR. But the use of high the high-bandwidth required by distributed secondary control could compromise the MG robustness.

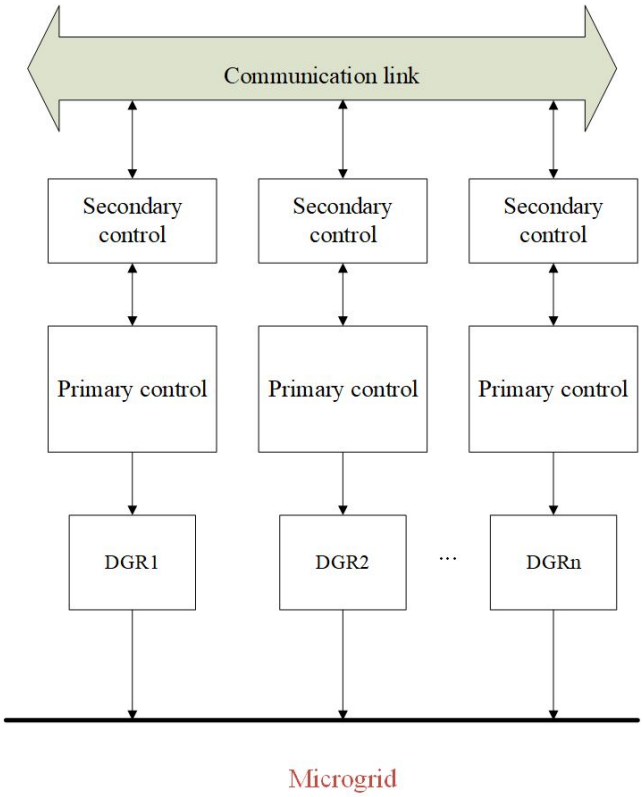

Figure 7.6 Distributed secondary control system for frequency regulation

Some efforts have been taken to mitigate the effect of communication link failures. Authors in [38] present a secondary control with no communications for islanded microgrids, where switches between two configurations according to a time-dependent protocol exist to archive frequency restoration. Event-trigger based secondary control methods are new approaches to reduce the communication band-width in [39]. Moreover, state estimation based secondary control strategy has been introduced to control voltage in MG [40].

Chapter 3：MG frequency control: modelling

3.1 Configuration of an islanded microgrid

3.1.1 Modelling of frequency response

Combing the renewable energy resource (e.g. solar power, wind power, water energy) with different energy storage systems in microgrid system, the generated electric power can meet the requirement of connected loads. Taking the model of the isolated MG system in thesis [41], which is shown in Figure 3.1. The MG system contains conventional diesel engine generator (DEG), PV panel, wind turbine generator (WTG), fuel cell (FC) system, battery energy storage system (BESS), and flywheel energy storage system (FESS). As shown in Figure 3.1, the DGs are connected to the MG by power electronic interfaces which are used for synchronization in ac sources like DEG and WTG and to reverse voltage in dc sources like PV panel, FC, and energy storage devices. The FC contains three fuel blocks, an inverter for converting dc to ac voltage and an interconnection device (IC). The FC has a high-order characteristic but a three-order model is sufficient for frequency studies [42]. Both FC and DEG are considered as parts of frequency secondary control to reduce the deviation.

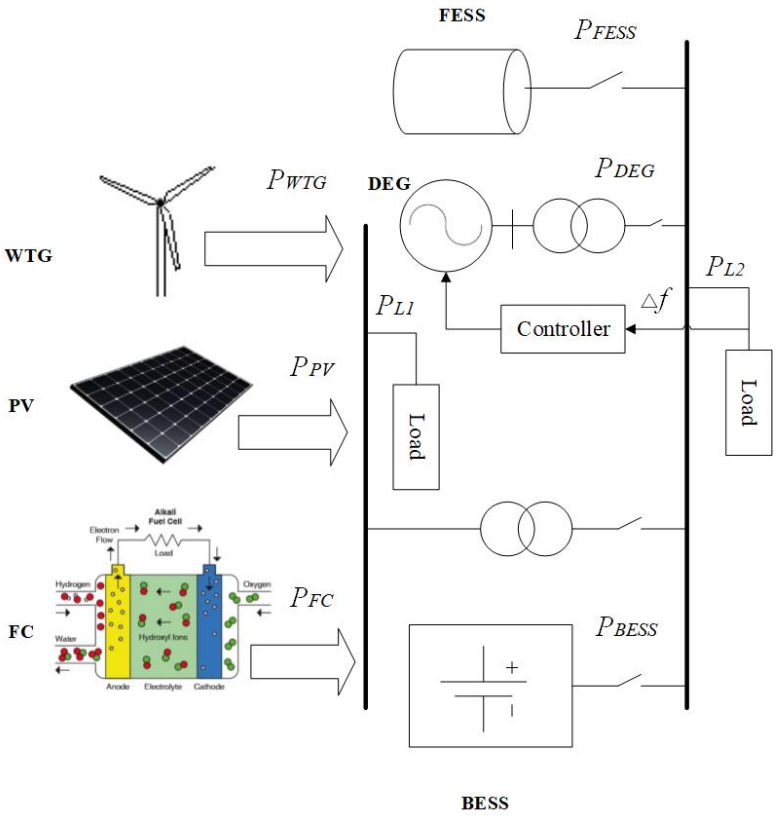

Figure 8.1 Single-line diagram of the ac MG

The circuit breaker is used in each microsource to disconnect from the network to avoid the impacts of severe disturbances through the MG or for maintaining purposes. Nominal values of the DG units and loads are given in TABLE I.

TABLE I RATED POWER OF DG UNITS AND LOADS

Rated power (KW)		Load (KW)	
WTG	100	P_{L1}	210
PV panel	30		
FC	70		
DEG	160	P_{L2}	210
FESS	45		
BESS	45		

The power balance function can be described as:

$$P_{LOAD} = P_{L1} + P_{L2} = P_{WTG} + P_{PV} + P_{FC} + P_{DEG} \pm P_{FESS} \pm P_{BESS} \tag{3.1}$$

where, the exchange power of FESS and BESS may be bilateral. FC and DEG are standby generators that deliver power to the system only when the total power generated by the WTG and PV is insufficient.

To precisely simulate the dynamic behaviors of practical WTG, DEG, FC, BESS, FESS, PV, etc., physical system must be extracted into mathematical model. For large-scale power system, however, simplified models or transfer functions are generally employed.

3.1.2 Characteristics of output power of WTG and PV

The output power of the studied wind turbine is determined by nondimensional curves of power coefficient C_p, which is a function of tip speed ratio λ and blade pitch angle β. The tip speed ratio can be defined by

$$\lambda = \frac{R_{blade}\omega_{blade}}{V_W} \tag{3.2}$$

where R_{blade}(=23.5m) is the radius of blades and ω_{blade} (=3.14 rad/s) is the rotational speed of blades. The function of C_p is given by

$$C_p = (0.44 - 0.0167\beta)\sin\left[\frac{\pi(\lambda - 3)}{15 - 0.3\beta}\right] - 0.0184(\lambda - 3)\beta \tag{3.3}$$

The output mechanical power of the mentioned WTG is

$$P_W = \frac{1}{2}\rho A_r C_p V_W{}^3 \tag{3.4}$$

where ρ (=1.25 kg/m^3) is the air density. A_r is the swept area of blades, which is 1735 m^2. V_W is the wind speed.

The output power of the studied PV system is characterized by

$$P_{PV} = \eta S \Phi \{1 - 0.005(T_a + 25)\} \tag{3.5}$$

where η is the conversion efficiency of the PV arrays, commonly ranging from 9% to 12%. S is the measured area of the PV array, Φ is the solar radiation and T_a is ambient temperature in degree Celsius. In this thesis, S=4084 m^2 and T_a is kept at 25 °C. Therefore, P_{PV} is linearly varied with Φ only.

3.1.3 The transfer functions of various generation subsystems

The transfer functions of the WTG, PV, FC, and DEG shown in Figure 3.1 are, respectively, represented as given:

$$G_{WTG}(s) = \frac{K_{WTG}}{1 + sT_{WTG}} = \frac{\Delta P_{WTG}}{\Delta P_W} \tag{3.6}$$

$$G_{PV}(s) = \frac{K_{PV}}{1 + sT_{PV}} = \frac{\Delta P_{PV}}{\Delta \Phi} \tag{3.7}$$

$$G_{FC}(s) = \frac{K_{FC}}{1 + sT_{FC}} \cdot \frac{1}{1 + sT_{IN}} \cdot \frac{1}{1 + sT_{I/C}} = \frac{\Delta P_{FC}}{\Delta f} \tag{3.8}$$

$$G_{DEG}(s) = \frac{K_{DEG}}{1 + sT_{DEG}} \cdot \frac{1}{1 + sT_t} = \frac{\Delta P_{DEG}}{\Delta f} \tag{3.9}$$

3.1.4 Transfer functions of different energy storage systems

Energy storage systems are essential to support insufficient energy of power generation subsystems of the microgrid system within a very short time to maintain system stability. Because the BESS takes time to charge energy to the battery cells or release the energy from the battery, its time constant is limited to several seconds. On the other hand, the FESS can store surplus energy during off-peak periods and quickly release energy during peak loads. The transfer functions of the BESS and FESS can be, respectively, expressed as a first-order lag as given next:

$$G_{BESS}(s) = \frac{K_{BESS}}{1 + sT_{BESS}} = \frac{\Delta P_{BESS}}{\Delta f} \tag{3.10}$$

$$G_{FESS}(s) = \frac{K_{FESS}}{1 + sT_{FESS}} = \frac{\Delta P_{FESS}}{\Delta f} \tag{3.11}$$

3.1.5 System frequency variation

In the autonomous microgrid system, the total power generation must meet the total power demand of the connected loads to maintain the stable operation. However, due to the difference ΔP_e between power demand reference P_d^* and total power generation P_g, the system frequency would wave. Hence, P-f control method mentioned in Chapter 2 is required to track the reference frequency.

$$\Delta P_e = P_d^* - P_g \tag{3.12}$$

The system frequency variation Δf is calculated by

$$\Delta f = \frac{\Delta P_e}{K_{sys}} \tag{3.13}$$

where K_{sys} is system frequency characteristic constant of the microgrid system. The transfer function for system frequency variation to per unit power deviation can be expressed by

$$G_{sys}(s) = \frac{\Delta f}{\Delta P_e} = \frac{1}{K_{sys}(1 + sT_{sys})} = \frac{1}{D + sM} \tag{3.14}$$

where D and M are, respectively, the equivalent inertia constant and damping constant [43].

3.2 Conventional PI controller

3.2.1 Frequency control model

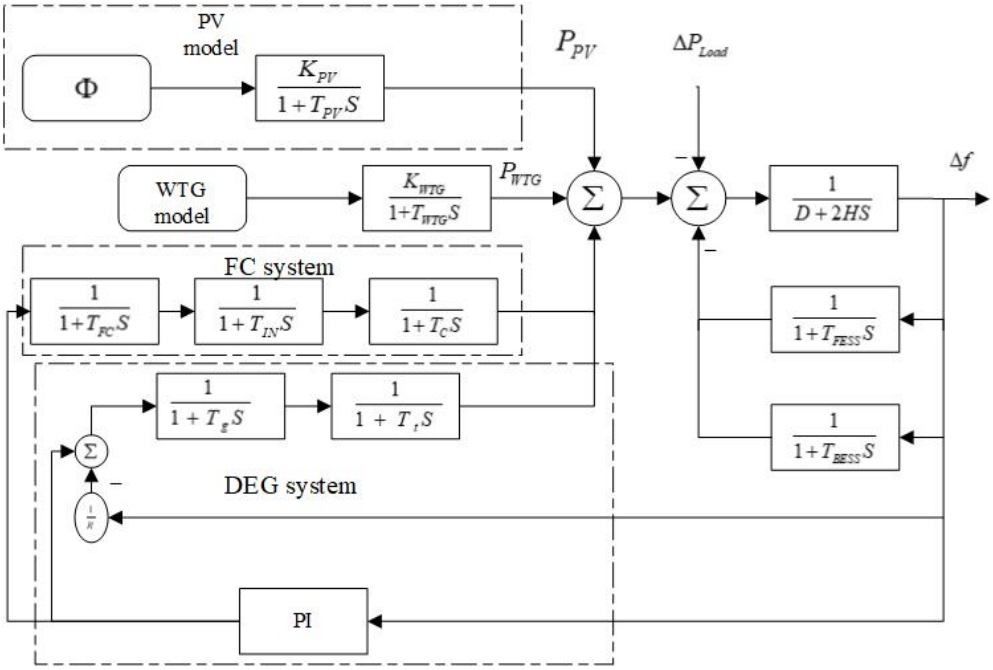

Figure 9.2 Conventional PI Frequency response model for the ac MG system

After modelling the microgrid frequency control system by transfer functions, a simplified frequency response model is shown in Figure 3.2. Parameter values of the block diagram of all following cases are given in TABLE II. Conventional frequency response model for the ac MG system is discussed where PI controller is responsible for the secondary control to compensate frequency deviation.

TABLE II THE PARAMETERS VALUES OF THE AC MG SYSTEM

Parameter	Value	Parameter	Value
D	0.015	T_g	0.08
2H	0.1667	T_t	0.4
T_{FESS}	0.1	T_C	0.004
T_{BESS}	0.1	T_{IN}	0.04
T_{FC}	0.26	R	3
K_{PV}	1	T_{PV}	1.8
K_{WTG}	1	T_{WTG}	1.5

3.2.2 WTG model and PV model

In this thesis, the total power of the connected loads for all simulation case study is assumed to be 1.0 pu under normal operating condition. And V_W is set to be 7.5 m/s and Φ is kept to be a smooth curve less than 0.3 pu. According to former assumptions, output of WTG and output of PV are depicted in Figure 3.3 and Figure 3.4.

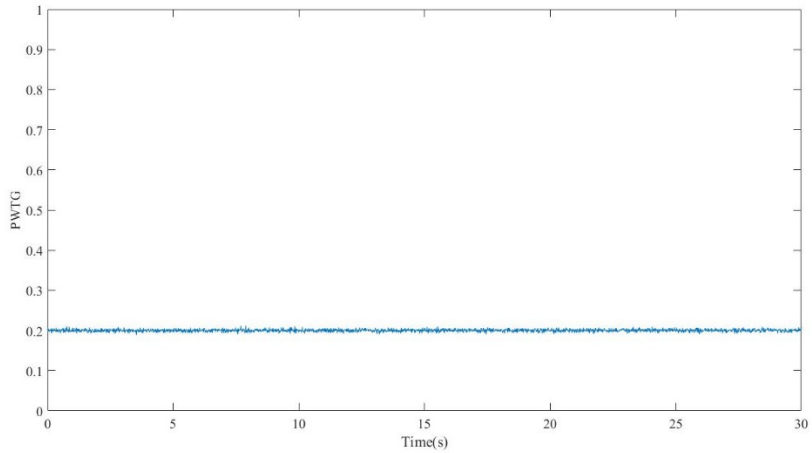

Figure 10.3 Wind turbine output

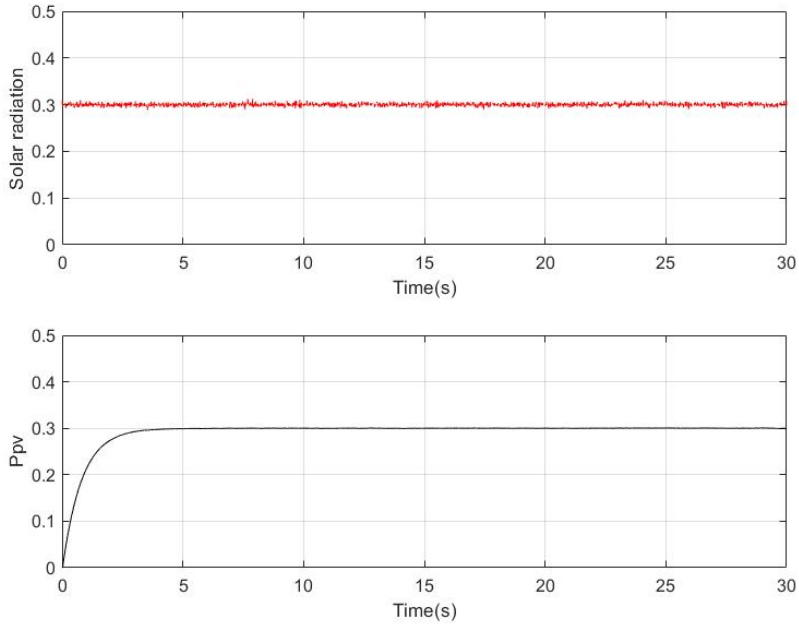

Figure 11.4 Solar radiation Φ and PV output power

It can be seen that the output of WTG and output of PV will remain stable under constant wind speed V_W and smooth Φ. Under the circumstance of little fluctuation of WTG output and PV output, this thesis would mainly focus on the frequency response under obvious load demand disturbance.

3.2.3 Simulation in Simulink

Simulink model of PI controller is shown as Figure 3.5.

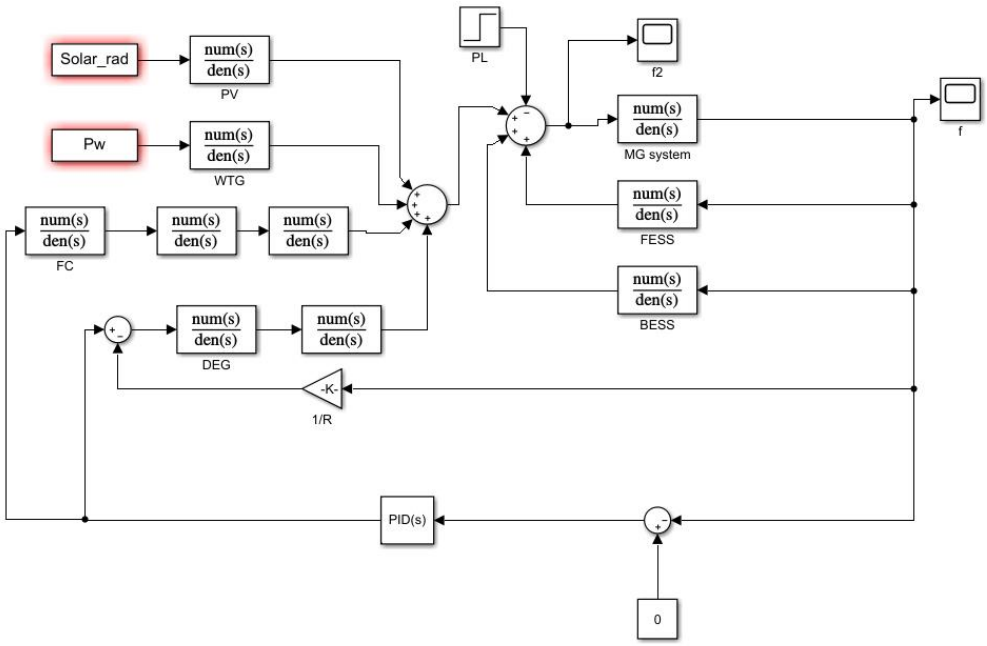

Figure 12.5 Simulink scheme-PI

To illustrate the dynamic response of the MG system, the closed-loop system is examined in the face of a multiple step load disturbance which is plotted in Figure 3.6 (a) and. And the system frequency response using conventional PI controller is shown in Figure 3.6 (b). Besides, conventional PI controllers are examined following a large step load disturbance of 0.1 pu as shown in Figure 3.7.

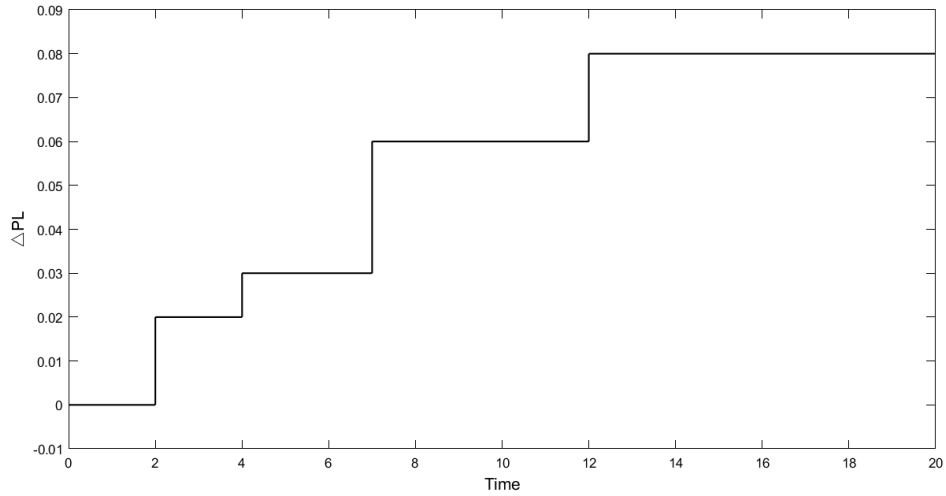

(a)

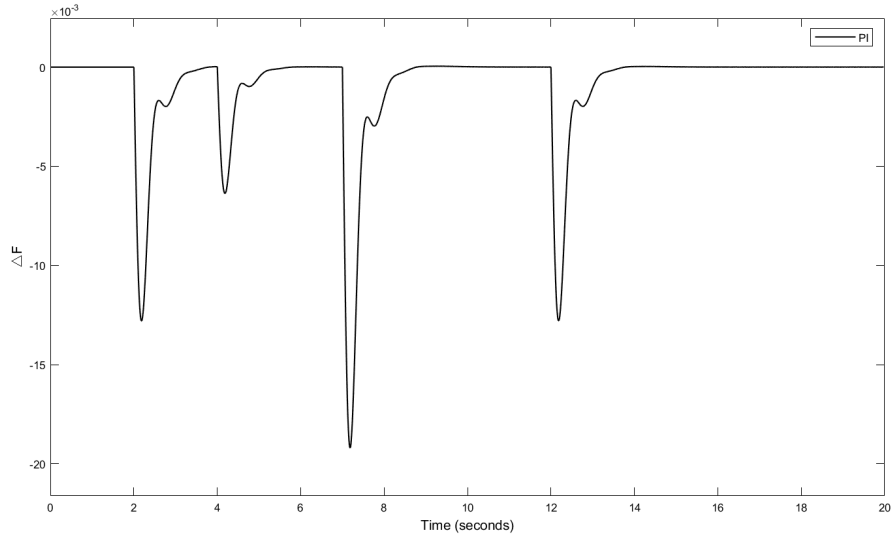

(b)

Figure 13.6 (a) Multiple step load disturbances (b) MG frequency response

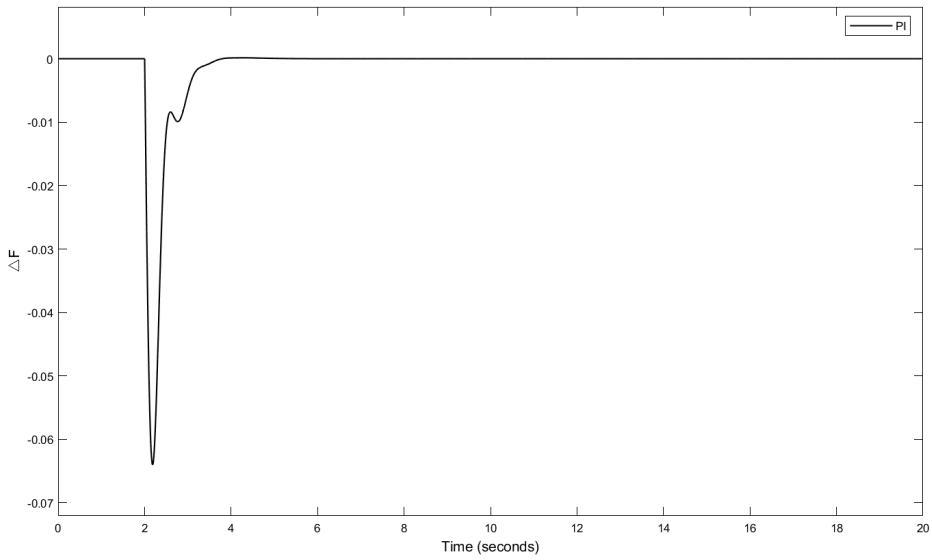

Figure 14.7 Frequency control following a step load disturbance of 0.1 pu

where, KP=0.3, KI=2. As shown in Figure 3.6 and Figure 3.7, the PI controller shows robustness and keeps the frequency stable from load disturbance no matter it's a single step disturbance or multiple step disturbances. The adjust time is less than 2 seconds. But the initial drop is still not satisfying, exceeding 0.05 pu.

In traditional power systems, the secondary frequency control is mostly done by conventional PI controllers that are usually tuned based on prespecified operating points. In

case of any change in the operating condition, the PI controllers cannot provide the assigned desirable performance. MPC can be used as a suitable intelligent method for online tuning of PI controller parameters and may get better performance.

3.3 Model predictive control

3.3.1 Principle of MPC

Model predictive control technology has been widely used in SISO, MIMO and nonlinear system [44-46]. MPC has serval advantages:1) handle the constraints in a systematic way, 2) admirable implement of considering nonlinear system, 3) calculation time can be reduced to get optimal control. The key feature of MPC is the model representation, which can be described as state space, transfer matrix or convolution type models. Depending on the model, computation and implementation will start automatically, processing the predicted value to make control decision. We assume the system to be discussed in state space by

$$x(k) = Ax(k-1) + Bu(k-1) \tag{3.15}$$

$$y(k) = Cx(k) \tag{3.16}$$

For zero-initial conditions, the equivalent transfer matrix representation is

$$y(z) = p(z)u(z) \tag{3.17}$$

$$p(z) = C(z\mathrm{I} - A)^{-1}B = \sum_{i=0}^{\infty} CA^{i}Bz^{-i-1} = \sum_{i=1}^{\infty} H_i z^{-i} \tag{3.18}$$

where H_i are the coefficients of impulse response. Thus, in the time domain, the output $y(k)$ can be calculated by

$$y(k) = \sum_{i=1}^{\infty} H_i u(k-1) \tag{3.19}$$

Then a cost function f_g is defined determine the optimal control behavior at a certain

time (control horizon). Depending on reference variable $x^*(t_{k+1})$ and predictive state variable $x_p(t_{k+1})$, f_g can be designed as $g_i = f_g\{x^*(t_{k+1}), x_p(t_{k+1})\}$. The common function is square of the difference between the reference variable and predictive state variable $g_i = \left\| x^*(t_{k+1}) - x_p(t_{k+1}) \right\|^2$. Naturally, control action which minimize the cost function is selected to control the system. In general, the most important part in MPC algorithm is the state estimation function, which directly influence the accuracy of predicted state values and may change the following control action.

3.3.2 MPC controller for MG frequency control

In this thesis, MPC controller is proposed to control the DEG and FC generation subsystem as a secondary control issue to maintain the stable frequency and power balance under disturbance of load demand, comparing with the conventional PI controller. The MPC framework for study is shown as Figure 3.8.

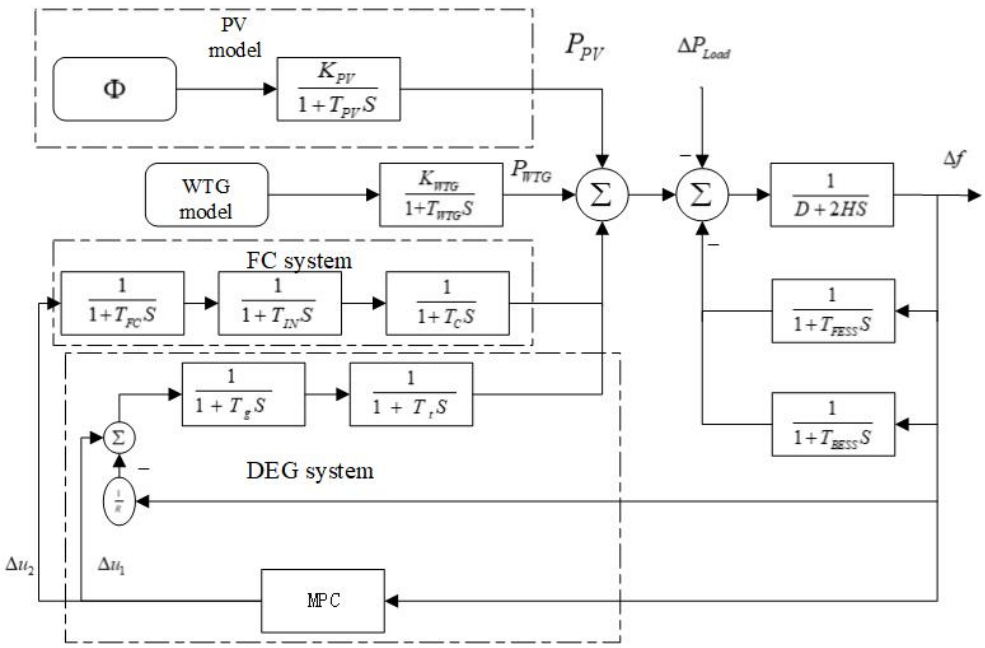

Figure 15.8 MPC framework

The goal is to control Δf which should be equal to zero. u is the output signal of MPC to change the power of FC and DEG.

The state space function of former system can be expressed as:

$$\begin{cases} \dot{x}(t) = Ax(t) + Bu(t) + F(\Delta P_{load} + \Delta P_{WTG} + \Delta P_{PV}) \\ y(t) = Cx(t) \end{cases} \tag{3.20}$$

$$x(t) = [\Delta f \;\; \Delta P_{DEG} \;\; \Delta \dot{P}_{DEG} \;\; \Delta P_{FC} \;\; \Delta \dot{P}_{FC} \;\; \Delta \ddot{P}_{FC} \;\; \Delta P_{FESS} \;\; \Delta P_{BESS}] \tag{3.21}$$

$$y(t) = \Delta f \tag{3.22}$$

$$u(t) = [\Delta u_1 \;\; \Delta u_2] \tag{3.23}$$

where

$$A = \begin{bmatrix} -\frac{D}{2H} & \frac{1}{2H} & 0 & \frac{1}{2H} & 0 & 0 & \frac{1}{2H} & \frac{1}{2H} \\ 0 & -\frac{1}{T_t} & \frac{1}{T_t} & 0 & 0 & 0 & 0 & 0 \\ -\frac{1}{RT_g} & 0 & -\frac{1}{T_g} & 0 & 0 & 0 & 0 & 0 \\ 0 & 0 & 0 & -\frac{1}{T_c} & \frac{1}{T_c} & 0 & 0 & 0 \\ 0 & 0 & 0 & 0 & -\frac{1}{T_{IN}} & \frac{1}{T_{IN}} & 0 & 0 \\ 0 & 0 & 0 & 0 & 0 & -\frac{1}{T_{FC}} & 0 & 0 \\ \frac{1}{T_{FESS}} & 0 & 0 & 0 & 0 & 0 & -\frac{1}{T_{FESS}} & 0 \\ \frac{1}{T_{BESS}} & 0 & 0 & 0 & 0 & 0 & 0 & -\frac{1}{T_{BESS}} \end{bmatrix} \tag{3.24}$$

$$B = \begin{bmatrix} 0 & 0 & \frac{1}{T_g} & 0 & 0 & \frac{1}{T_{FC}} & 0 & 0 \end{bmatrix} \tag{3.25}$$

$$C = [1 \;\; 0 \;\; 0 \;\; 0 \;\; 0 \;\; 0 \;\; 0 \;\; 0] \tag{3.26}$$

$$F = [-\frac{1}{2H} \;\; 0 \;\; 0 \;\; 0 \;\; 0 \;\; 0 \;\; 0 \;\; 0] \tag{3.27}$$

and Δf , ΔP_{DEG} , ΔP_{FC} , ΔP_{FESS} , ΔP_{BESS} , ΔP_{load} are the deviation of frequency, the DEG system output, the FC system output, the FESS system output, the BESS system output and load, respectively. Δu_1 and Δu_2 are control signals from controller.

Cost function

$$J(N_1,N_2,N_u)=\sum_{j=N_1}^{N_2}[\Delta\omega(t+j|t)-0]^2+\lambda_1\sum_{j=0}^{Nu}[\Delta u_1(t+j-1)]^2+\lambda_2\sum_{j=0}^{Nu}[\Delta u_2(t+j-1)]^2 \quad (3.28)$$

The first term minimizes the tracking error between the prediction of the measured system frequency and its set-point ω_n, and the second term minimizes the control action effort. λ_1,λ_2 are weighting factor value, which in this thesis have been selected to obtain similar SCS bandwidth for MPC to that achieved for the other SCS strategies studied in this thesis. N_1,N_2 are the minimum and maximum costing horizons, respectively, and N_u is the control horizon. $\Delta u_1,\Delta u_2$ are control signals processed by MPC.

Then, MPC controller can be given by

$$U=-KX \quad (3.29)$$

The MPC Simulink scheme is shown as Figure 3.9.

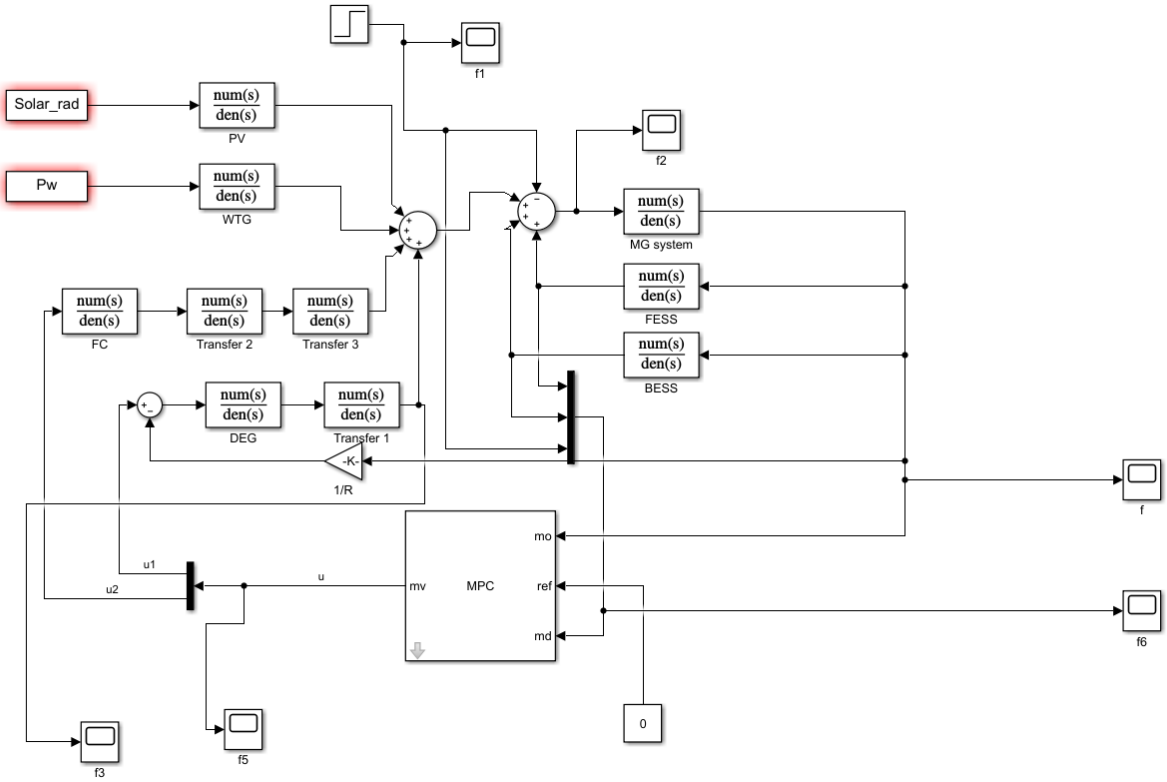

Figure 16.9 Simulink scheme-MPC

3.4 Case study

Power system operation states are changing in the real-time situation, which may degrade the performance of the closed-loop microgrid system, distressingly. As indicated in the previous sections, one of the main advantages of the advanced control methods is robustness against environmental and dynamical changes. To illustrate the robustness of MPC control strategy, three cases based on the different conditions of BESS and FESS are designed. In the meanwhile, the simulation result of MPC controller will be compared with PI controller mentioned before.

3.4.1 Case design

Microgrid can operate in both grid-connected and islanded operating modes to avoid huge loss caused by external faults. The control schemes for MG system in islanded mode are more complex and important than that in grid-connected mode; hence, an isolated ac MG system is considered as a case study in this thesis. In addition, the changing state of FESS and BESS may degrade the closed-loop system performance. Therefore, two binary variables S_{FESS}, S_{BESS} are proposed to describe the statuses of FESS and BESS system. If $S_{FESS}, S_{BESS} = 0$, the energy storage systems operate in idle mode which means they reach their maximum capacity limit and they can't release or charge power furthermore at that status. And if $S_{FESS}, S_{BESS} = 1$, the energy storage systems operate in connected mode with ability to respond to the dynamic change of load power. According to the combination of those two variables, there are supposed to be 4 cases. However, due to the same transfer function of FESS and BESS, there are three cases shown as TABLE III.

TABLE III CASE STUDY DESIGN

Case study	S_{FESS}	S_{BESS}
Case1	1	1
Case2	0	0
Case3	1	0

3.4.2 Simulation result and discussion

Case1:

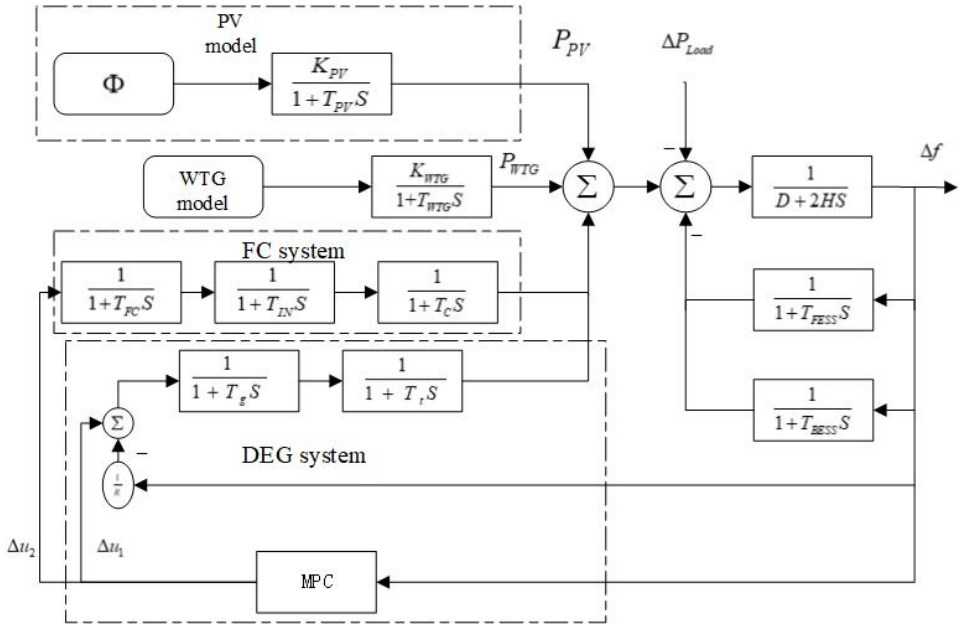

Figure 17.10 Case1 control system scheme

The block diagram of this studied case is shown as Figure 3.10. WTG and PV as renewable sources are combined with DEG, FC, FESS and BESS. Power inverters are properly used in various generation systems and energy storage systems to realize dc-ac transform. The frequency error sign will be sent to both FC and DEG, processed by MPC controller to respond to dynamic change of the connected load power. Assume that FC and DEG have their own

MPC controller which means distributed control strategy, operating with others to obtain better performance. In this case, uncertainty for the parameters which would influence the output of WTG and PV generation is not considered. Besides, we assume that FESS and BESS have no limit and they have enough capacity to store or release power in the system. Thus, they may have faster speed for processing the frequency error signal produced by ΔP_{Load}. So output signals from BESS and FESS function are negative, to a certain degree, like a simple droop control.

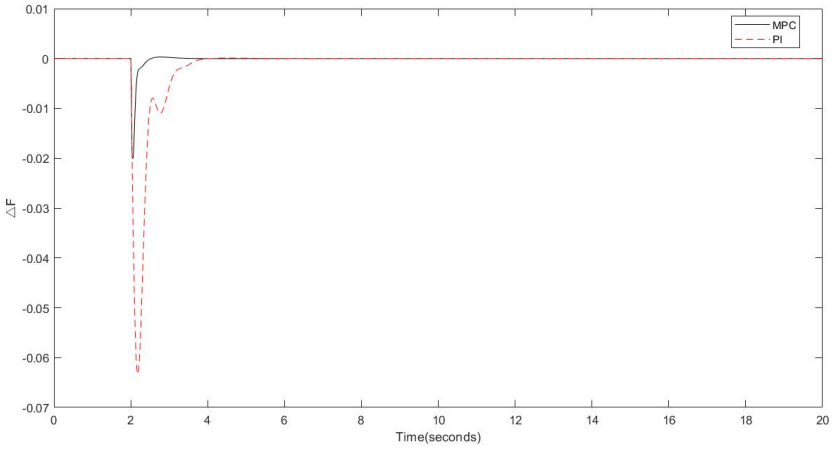

Figure 18.11 Frequency control following a step load disturbance of 0.1 p.u

There are two separate control signals from MPC sent to FC and DEG system to produce corresponding power. The cooperation of two manipulated signals from MPC can obtain better performance with less adjustment time.

where, sampling time is 0.01s, prediction horizon is 80 steps, control horizon is 4 steps, λ_1=0.1, λ_2=0.1.

The frequency response is shown as Figure 3.11.

Case2:

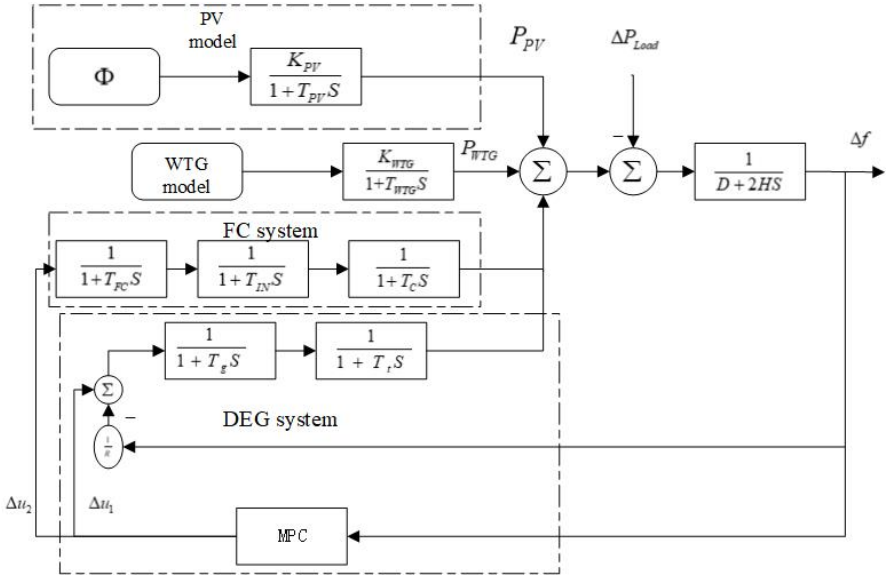

Figure 19.12 Case2 control system scheme

The block diagram of this studied case is shown as Figure 3.12. WTG and PV as renewable sources are combined with DEG, FC. Power inverters are properly used in various generation systems and energy storage systems to realize dc-ac transform. The frequency error sign will be sent to both FC and DEG, processed by MPC controller to respond to dynamic change of the connected load power. Assume that FC and DEG have their own MPC controller which means distributed control strategy, operating with others to obtain better performance. In this case, uncertainty for the parameters which would influence the output of WTG and PV generation is not considered. Unlike case1, FESS and BESS lose their ability to respond ΔP_{Load} at high speed. In other words, they may just communicate with WTG and PV to charge or release power directly. So BESS and FESS function can be removed in simulation.

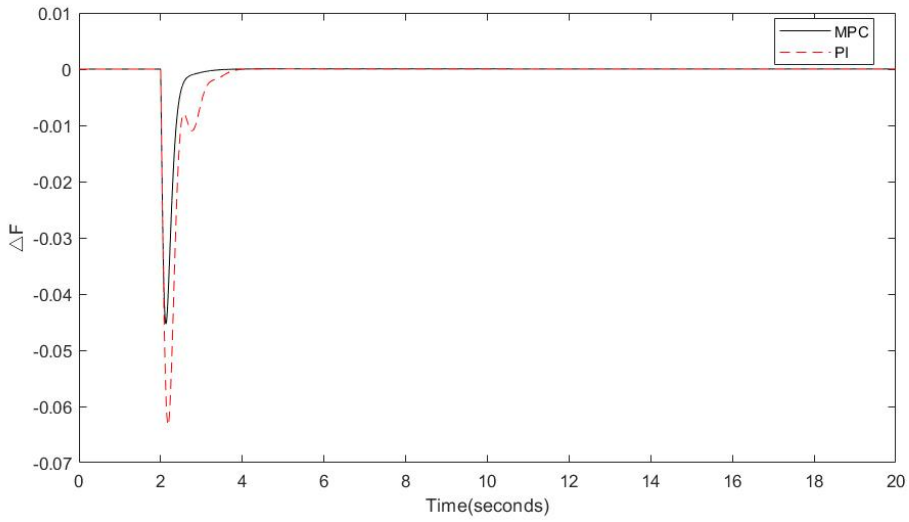

Figure 20.13 Frequency control following a step load disturbance of 0.1 p.u

The frequency response is shown as Figure 3.13.

Case3:

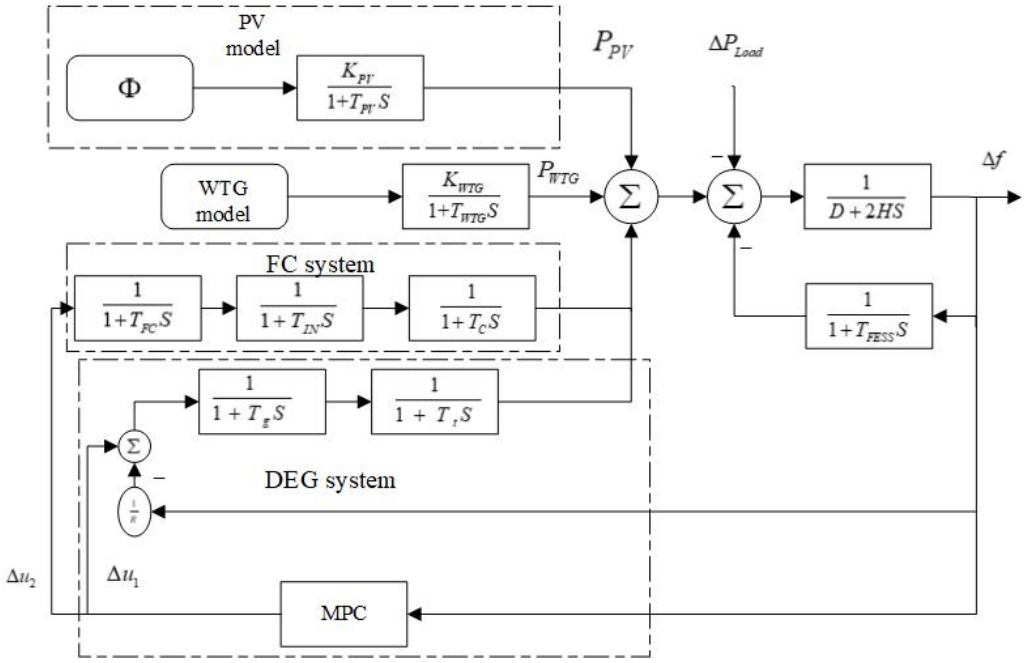

Figure 21.14 Case3 control system scheme

The block diagram of this studied case is shown as above. Almost part of this case is the same as case1 while the BESS are removed from the system. The FC and PV may generate dc power that is converted into ac power using a dc–ac power converter. Again, the FESS have no

limit and they have enough capacity to store or release power in the system.

The frequency response is shown as Figure 3.15.

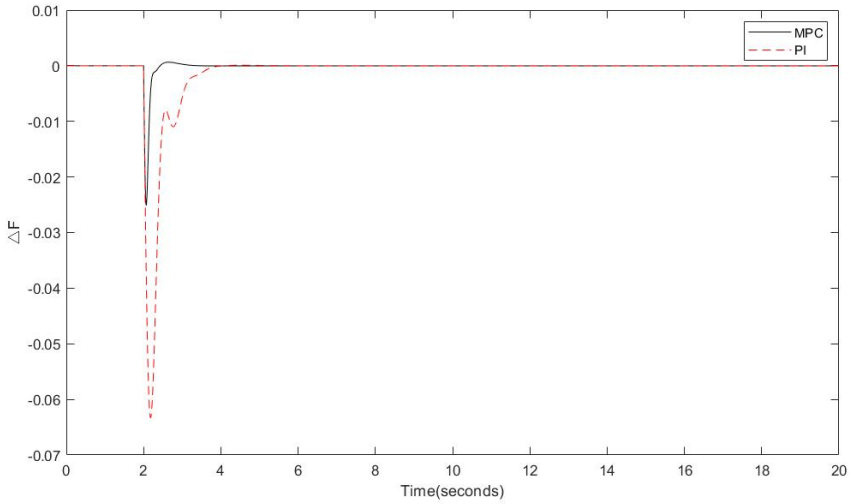

Figure 22.15 Case 3 frequency control following a step load disturbance of 0.1 p.u

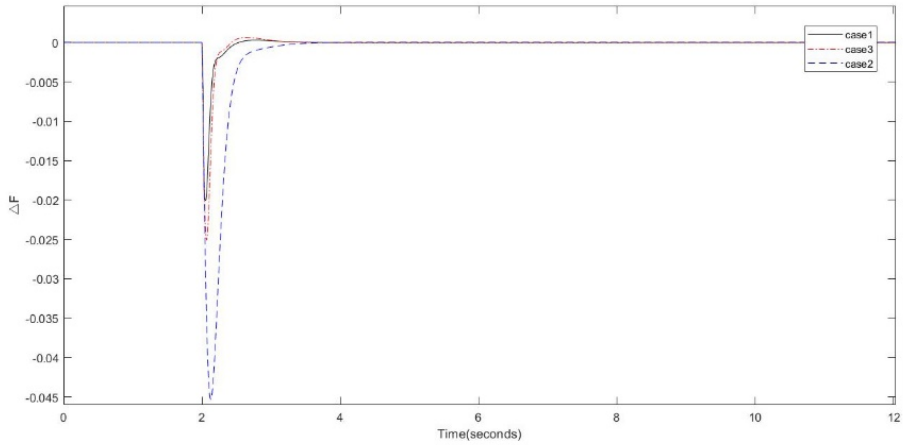

Figure 23.16 Comparison for three cases

From Figure 3.11, Figure 3.13 and Figure 3.15, we can find that the MPC controller has less overshoot and fast response speed. Frequency deviation in three case for MPC controller are all less than 0.05 pu, reaching the desirable operation demand. It can be seen clearly that case 1 has the best performance from Figure 3.16, since BESS and FESS have the ability to supply insufficient generation subsystem within a short time. Besides, when BESS and FESS

loss their responsible ability, there is little difference between PI control method and MPC control method (seen as case 2). In summary, through case study, it shows the advantage of MPC control strategy in microgrid frequency control system and confirms its robustness under dynamic change.

Chapter 4: MPC status feedback attack

4.1 Attack description

As mentioned in Chapter 3, various status feedback of FESS and BESS S_{FESS}, S_{BESS} may contribute to different performances of the closed-loop system. Due to the same transfer function of FESS and BESS, there are three conditions related to the status of FESS and BESS, illustrating whether they are connected to the system or not. All three conditions can achieve frequency regulation, but the overshoot and response speed are totally different as they can be distinguished easily. State estimation based on accuracy status feedback of the system components is essential for the MPC controller to calculate corresponding control signal. If status feedback of BESS and FESS are attacked by adversary, it may degrade the performance of power system, causing huge of losses. For example, only BESS is available when the load demand increases which means $S_{FESS}=1, S_{BESS}=0$. However, after attacks is implemented in MPC, the state estimator would receive the wrong information that both of FESS and BESS are still on work to handle the power unbalance, which means $S_{FESS}=1, S_{BESS}=1$. It may lead to risky control strategy and terrific performance of system operation, producing impacts on reliability and security of power grid. The scheme under MPC status feedback attack is depicted as Figure 4.1.

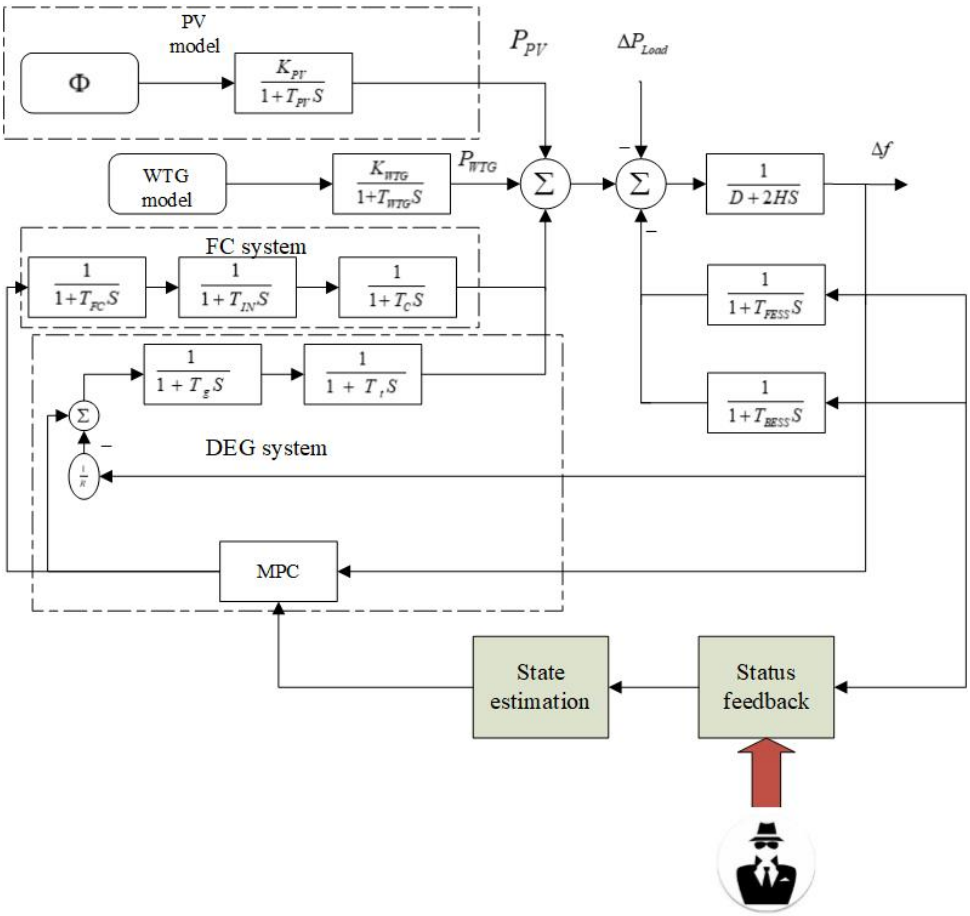

Figure 24.1 Scheme of MPC status feedback attack

From Figure 4.1, we can see that the hacker may get the access to attack state estimation of MPC by injecting false data. Actually, the status feedback of WTG, PV, DEG and FC all can be attacked. For simplicity, we only consider the attack to the statuses of FESS and BESS. Further detection and online switching from different conditions are required to address status feedback attack. We assume that if the frequency deviation is found to be different from what it supposed to be, the state space of the system can be modified immediately. Then we need to classify the actual situation among above three cases. New calculation and optimization progress would be done automatically after the accuracy state space function and current states of each components in the system are taken by the MPC controller.

4.2 Online switching method

Due to different statues of BESS and FESS, the state space functions that describe the dynamic model of mentioned microgrid system vary from one to the other. Only with the accuracy state space function, the state estimation can be processed properly, and the deviation of frequency can be regulated. As the historical data of MPC output control signal u are known, the estimated frequency deviation of former three situations (S_{FESS}=0,S_{BESS}=0 , S_{FESS}=1,S_{BESS}=0 , S_{FESS}=1,S_{BESS}=1) can be obtained. Euclidean metric is proposed to measure the relativity of current frequency deviation and the estimated frequency deviation. If we compare current data and mentioned estimated data, we can detect the statuses of BESS and FESS where the less error one can be recognized as actual statuses. Status feedback attack online detection block is shown as Figure 4.2.

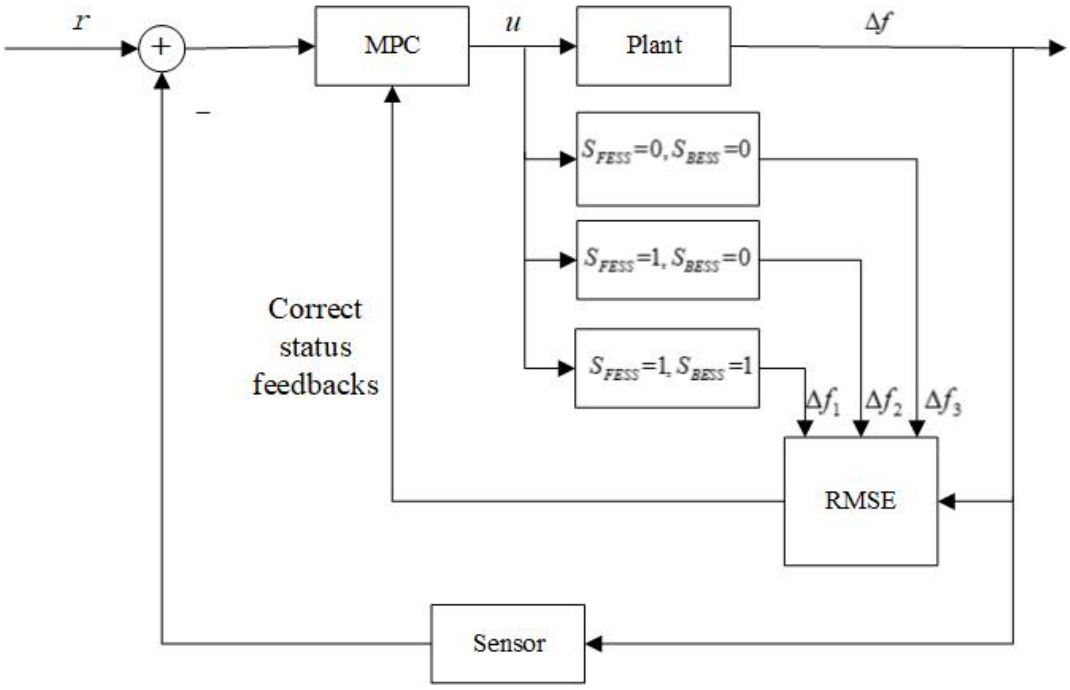

Figure 25.2 Status feedback attack online detection block

Although the state estimation is hacked by adversary at first, which may lead to terrific

performance of system operation, a status feedback attack online detection is proposed to address this problem. According to the state space function of each situation shown as status block in Figure 4.2, $\Delta f_1, \Delta f_2, \Delta f_3$ can be calculated respectively during specific observation time. Then RMSE (Root Mean Squared Error) block is utilized to measure the error when comparing $\Delta f_1, \Delta f_2, \Delta f_3$ with Δf. Then the less error one is approximately considered as current updated status feedback of BESS and FESS. Therefore, the MPC controller is modified by updated status feedback in real time. In next control step, predicted states and control signal are computed by the updated state space function of actual model related to statuses of BESS and FESS.

4.3 Case study

In this case, FESS and BESS system are in idle mode ($S_{FESS}=0, S_{BESS}=0$) which means they reach their maximum capacity limit and they can't release or charge power furthermore at that status. However, the state estimations of FESS and BESS system are hacked by the intruder, resulting the status feedback from BESS and FESS to be $S_{FESS}=1, S_{BESS}=1$. As the MPC controller takes the wrong status feedback, control signal would be totally different from what it should be in the regular operation. Therefore, inevitable damage and insufficient control function may be occurred in the respect of dynamic model of frequency secondary control based on MPC.

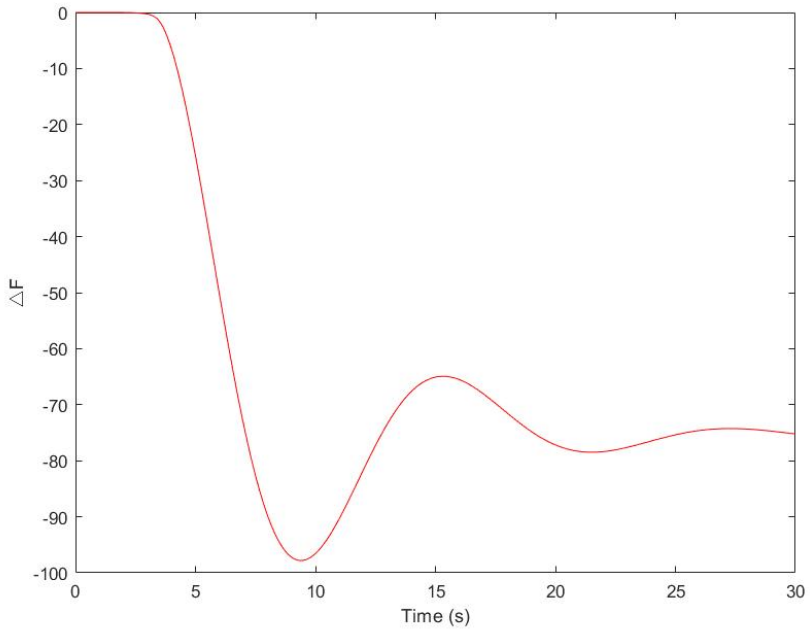

Figure 26.3 Frequency response under status feedback attack

The frequency response of mentioned case with 0.1 pu load disturbance at t=2s is depicted as Figure 4.3, which is simulated in MATLAB. It can be seen that such status feedback attack would cause system instability and slightly obtain the expectation of frequency control.

Then, the proposed online detection and switching method with 0.1 pu load disturbance at t=2s is implemented in simulation. The result of system frequency response and online detection of statues of BESS and FESS are shown as Figure 4.5 and Figure 4.6, respectively. From Figure 4.4 and Figure 4.5, we can verify the effectiveness of the proposed method to achieve frequency regulation with the MPC controller as secondary control part. In Figure 4.6, when t=2.05s, the algorithm can detect the accuracy status feedback of FESS and BESS, where BESS, FESS=00 represents $S_{FESS}=0, S_{BESS}=0$. Therefore, the MPC controller can modify the state estimation with the original states of FESS and BESS.

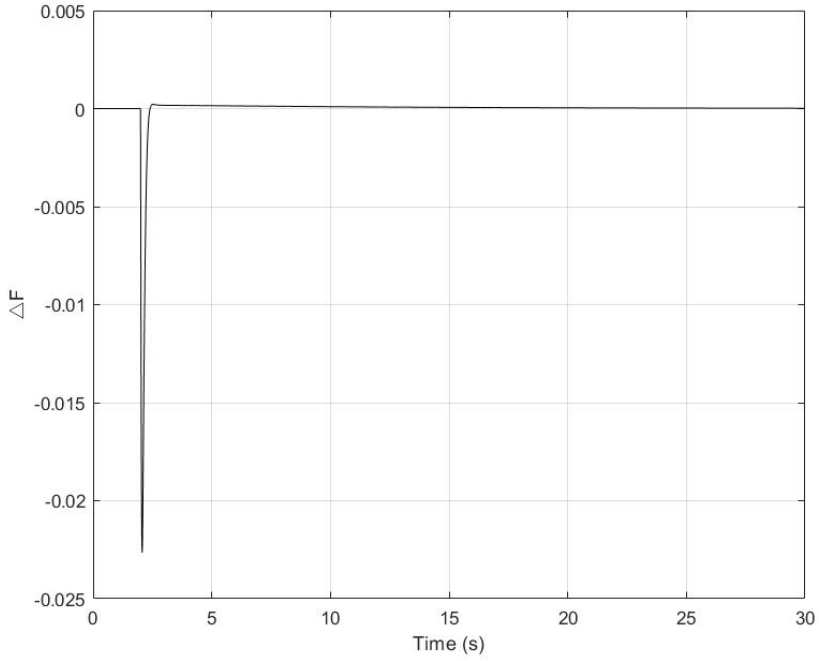

Figure 27.4 Frequency response with online switching method under status feedback attack

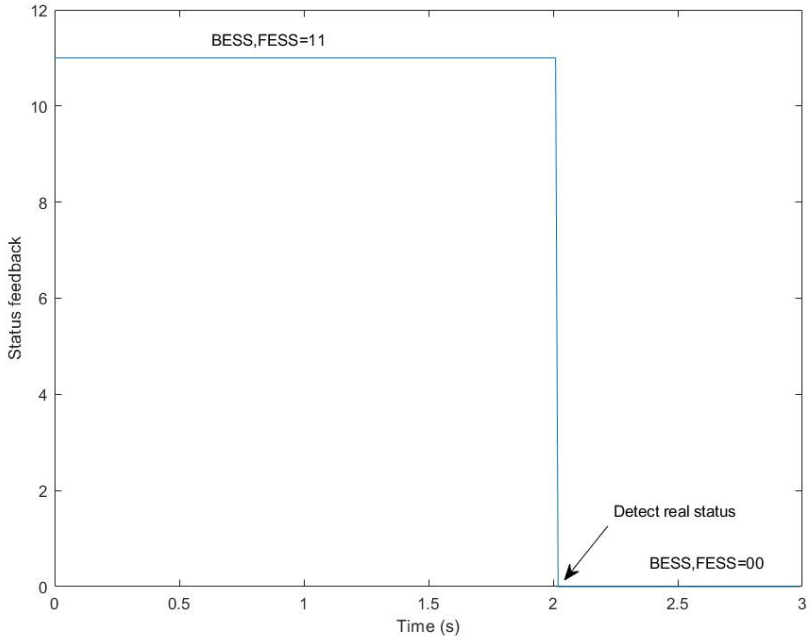

Figure 28.5 Online detection of statues of BESS and FESS

Chapter 5: Modified MPC controller under time-delay attack

5.1 Time delay attack

Modern power grids rely on open communication infrastructure to improve the efficiency, sustainability and reliability of three levels of power system (generation, transmission and distribution), which makes them vulnerable to cyber-attacks implemented by adversary. In general, an intruder attempts to get into IT infrastructure of control system and manipulate various sensors to disrupt control signals. For example, an intruder can shut down a load on a specific power transformer or introduce inefficiencies in the power supply.

Many efforts have culminated in a huge number of literature, including stability analyzing method of attacks on industrial control systems, updating hardware and software systems and advanced measurement units to prevent potential attacks from destroying secure operation. An identifying method for a change in sets of inferred candidate invariants under FDI attack is proposed in [47]. Literature [48] studies the impact of FDI on distributed load sharing. In [49], Markov based state transition rules is presented to simulate microgrid responses considering the behavior of PV and ESS control systems. Authors in [50] consider how a time-delay attack affects the dynamic performance of a power system.

Commonly, the local information measured by sensors is sent to the communication channel. Then state estimator starts to calculate current states which is essential for making control decision in control center. After receiving the signal from control center, frequency controller can send the control signal to all kinds of DEG through the communication channel. Due to the high dependence of communication infrastructure, the system would be vulnerable

to various attack risks. A simplified load frequency control system under time-delay attack is depicted in Figure 5.1. However, most of recent studies considered either the construction of controllers that are robust to time delays or controllers that train offline with a time-delay function for estimation. As far as it is known, there are few control methods that perform online estimation of dynamic time delays and real-time control of power systems.

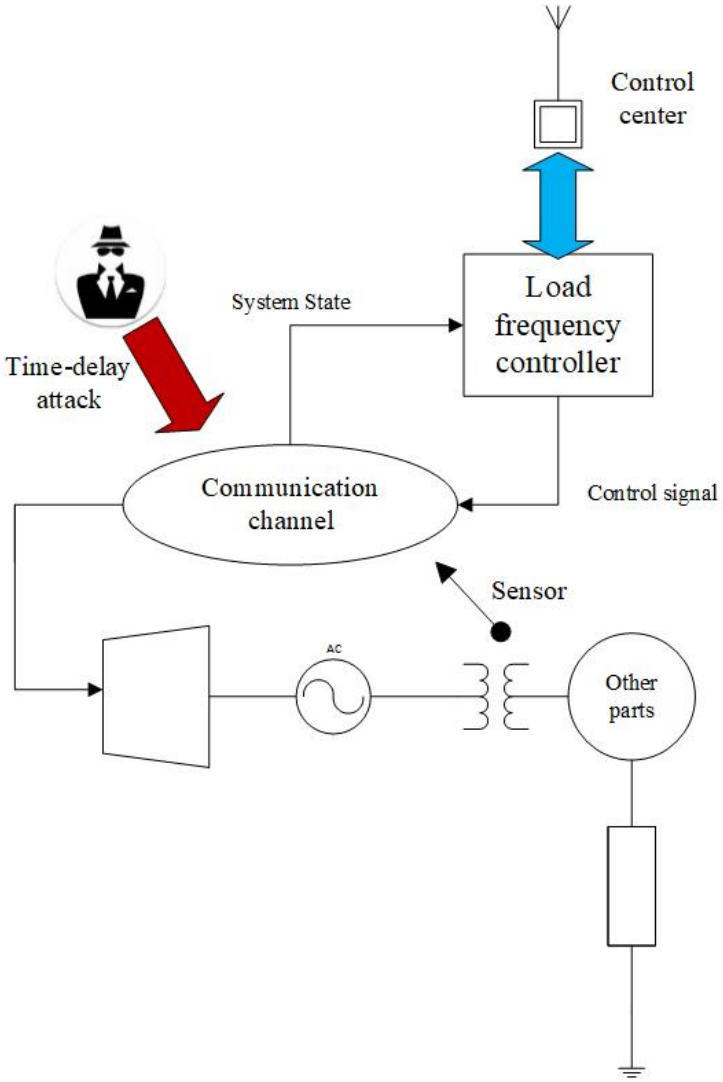

Figure 29.1 A simplified load frequency control system under time-delay attack

5.2 MPC controller under time-delay attack

5.2.1 Modelling

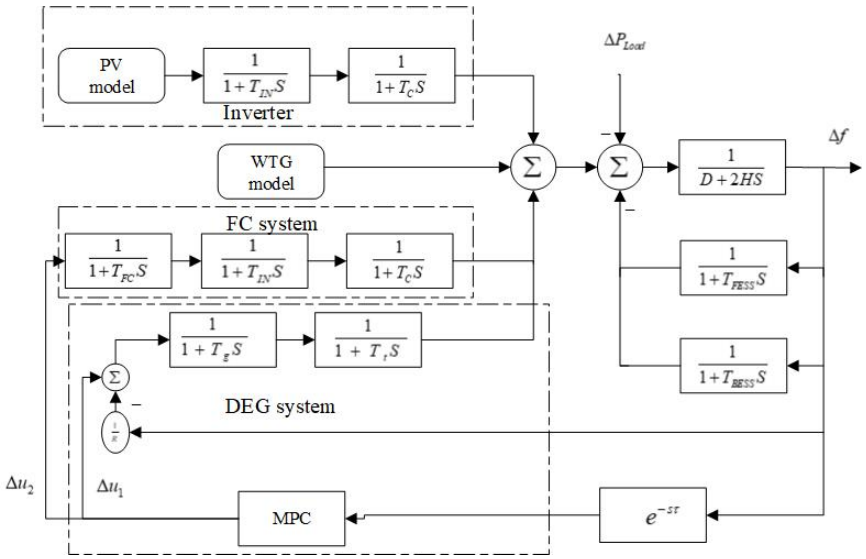

Figure 30.2 Dynamic model of MPC frequency control with delay attack

The model of conventional MPC control scheme is modified, shown in Figure 5.2, considering the time delay attack in the control loop.

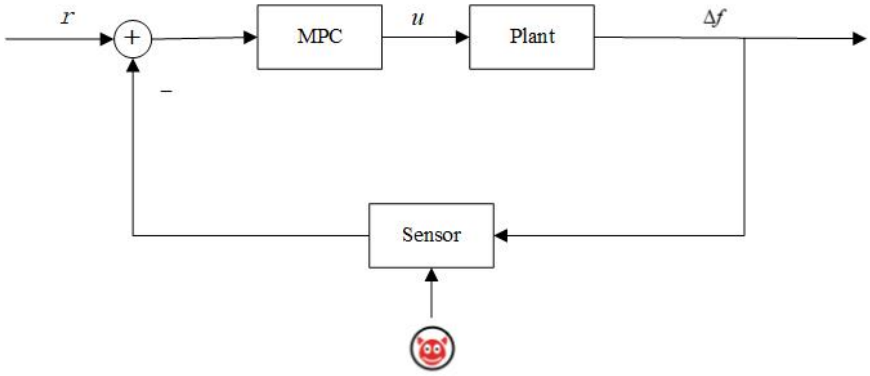

Figure 31.3 MPC control block diagram under attack

The deviation of frequency of plant output, which is detected by sensor (PLL in microgrid), will be compared to reference signal *r*. However, the sensed data will be delayed due to time-delay attack, causing different state estimation of MPC controller. Then the control signal *u* is

not corresponding to real system state, and fluctuation of frequency and undesirable performance would occur.

The state space function of former system can be expressed as same as formula 3.20. Besides, as shown by an exponential block $e^{-s\tau}$, τ is the estimated time delay of the system. With the time-delay attack, the control signal will be modified by

$$U = -K\hat{X} \tag{5.1}$$

And the new state after attack can be modeled by

$$\hat{X} = \begin{bmatrix} \hat{x}_1 \\ \hat{x}_2 \\ \vdots \\ \hat{x}_8 \end{bmatrix} = \begin{bmatrix} x_1(t-\tau_1) \\ x_2(t-\tau_2) \\ \vdots \\ x_8(t-\tau_8) \end{bmatrix} \tag{5.2}$$

Since a time-delay attack can sabotage and ruin the network control system to cause huge loss, control strategies must be developed that must be able to detect and track the time-delay attack and manage a response strategy.

5.2.2 Case study with known time-delay signal

In this case, time delay τ is assumed to be known in system. Under four different delay time and 0.1 pu load disturbance at 2s, the frequency respond of microgrid system with MPC controller is shown as Figure 5.4, Figure 5.5, Figure 5.6 and Figure 5.7.

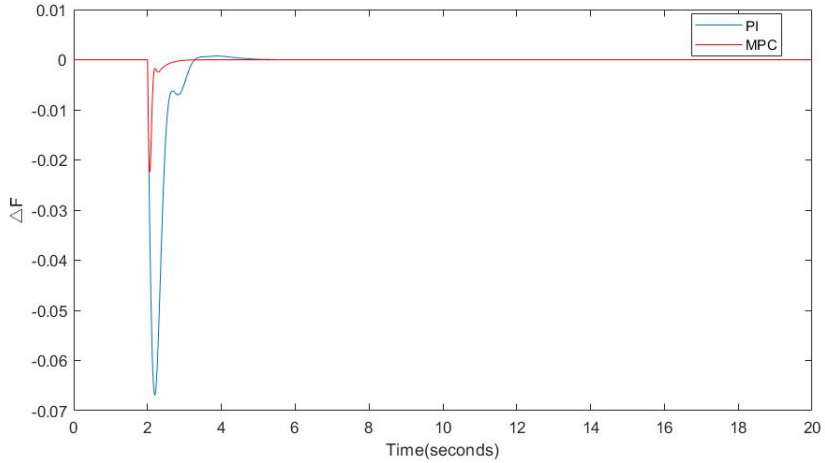

Figure 32.4 Frequency respond when τ =0.1s

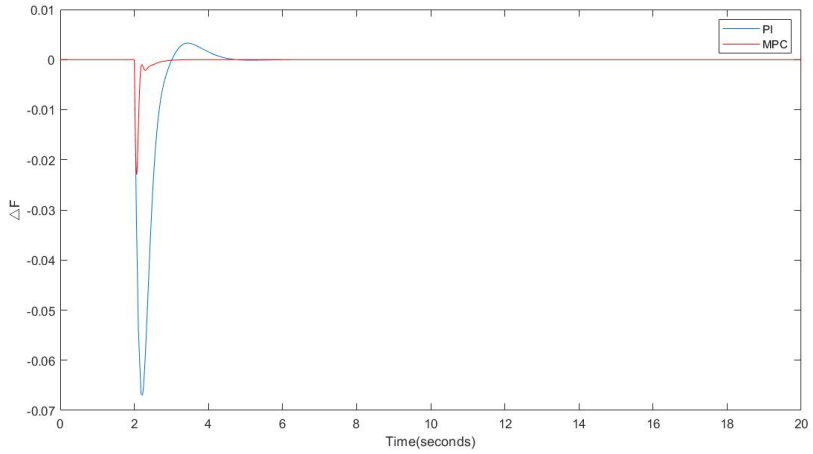

Figure 33.5 Frequency respond when τ =0.2s

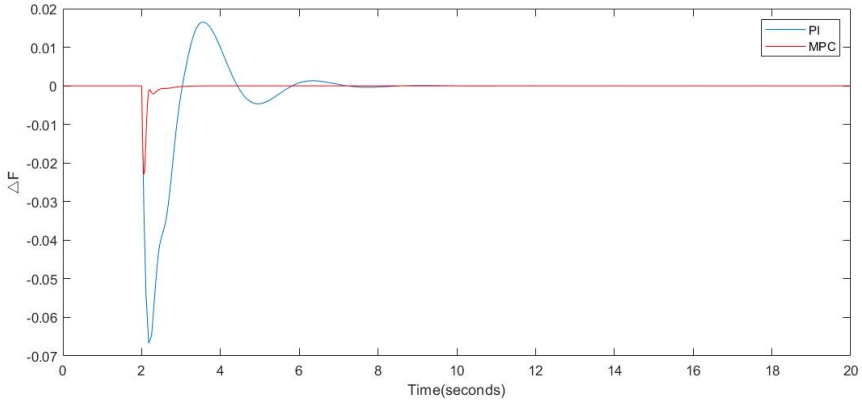

Figure 34.6 Frequency respond when τ =0.4s

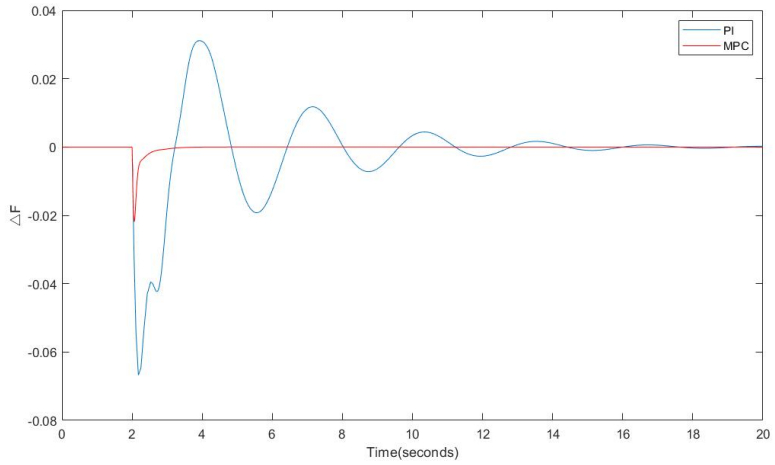

Figure 35.7 Frequency respond when τ =0.6s

where, sampling time is 0.01s, prediction horizon is 80 steps, control horizon is 4 steps, λ_1=0.1, λ_2=0.1.

It can be seen clearly that MPC controllers will obtain better performance (less overshoot, faster adjust time, stable curve) of microgrid frequency control than PI controllers with increasing delay time. Even when τ is larger than 0.6s, the frequency respond of PI controller will be divergent. Under the situation of known time-delay, MPC controllers are promising. However, in the real power system, it's impossible to get the exact information of time-delay attack by adversary instant immediately, or time-delay attack can be time-varying. Therefore, it's indispensable to set up a new algorithm to prevent time-delay attack on microgrid frequency control system in real-time.

5.3 Modified MPC with online time-delay estimation

5.3.1 Methodology

The new method involves the use of the plant model, a time-delay estimator, and the MPC controller to control system frequency under TDS attack. The control scheme will detect and track time delays introduced by a hacker and guide the plant to track the reference signal to guarantee the stability for the system. Figure 5.8 shows the diagram of proposed control method.

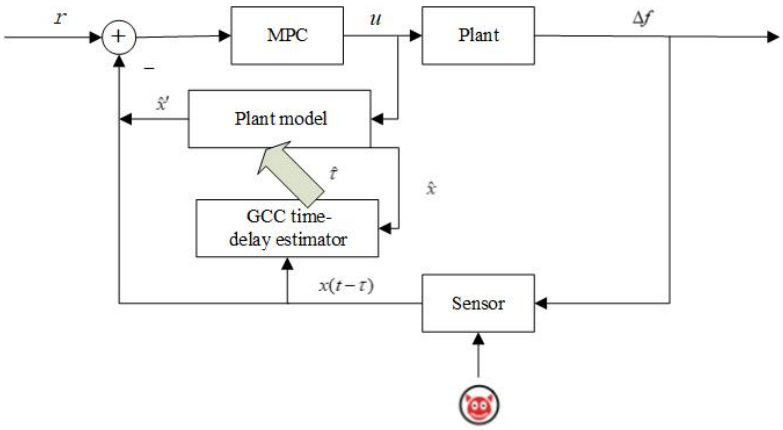

Figure 36.8 Block diagram of proposed control technique

This thesis proposes a GCC (generalized cross correlation) time-delay estimator to update delay estimation. Then the state space can be modified with estimated time-delay. According to the updated plant model, MPC controller could adjust their control signal to eliminate the fluctuation caused by unknown delay attack.

For simplification, the system being dealt with can be approximated in state space function, which takes plant block directly to describe the dynamic of system.

$$\Delta\dot{f}(t) = \dot{x}(t) = Ax(t) + Bu(t) \tag{5.3}$$

and its solution is given by

$$x(t) = e^{At}x_0 + \int_0^t e^{A(t-s)}Bu(s)ds \tag{5.4}$$

Due to the time-delay attack from the attacker, the solution becomes

$$x(t-\tau) = e^{A(t-\tau)}x_0 + \int_0^{t-\tau} e^{A(t-\tau-s)}Bu(s)ds \tag{5.5}$$

In general, the time delay τ is an unknown variable. No matter it is a constant or time-varying value, we want to estimate the time delay τ.

It should be noted that $x(t-\tau)$ is actually measured from sensor. So, at every instance of time, variable $u(t), A, B$ and $x(t-\tau)$ are known to the controller and the plant model. On the other hand, the current $x(t)$ and the time delay are unknown. It is essential to estimate the time delay τ firstly and then estimates $x(t)$ correctly.

Assume that former state can be obtained at every time step. The plant model estimation equation is given by

$$\dot{\hat{x}}(t) = A\hat{x}(t) + Bu(t) + F\Delta P_{load} \tag{5.6}$$

Through the plant model estimation, we can calculate the estimated state value $\hat{x}(t)$ since $A, B, F, \Delta P_{load}$ are known and former $u(t)$ processed by MPC controller are saved. Then, GCC estimator can be used to estimate time delay τ by comparing $\hat{x}(t)$ and $x(t-\tau)$. So it's definitely important to get the plant model state estimation in order to estimate time delay attack to the communication channel.

5.3.2 Generalized cross correlation

GCC algorithm is widely used in field of signal processing to estimate the time delay between two signals [51-52]. In some sense, the output signal from sensors and state estimate

signal are two related signals, which can also use GCC to detect and track time delay.

For convenient, $\hat{x}(t)$ and $x(t-\tau)$ can be mathematically remarked as

$$y_1(t) = x(t-\tau) = s_1(t) + n(t) \tag{5.7}$$

$$y_2(t) = \hat{x}(t) = s_1(t+D) \tag{5.8}$$

where $s_1(t)$ is real signal obtained from sensor, $n(t)$ is noise signal. Signal $s_1(t)$ is assumed to be uncorrelated with $n(t)$.

Here, the cross-correlation function is proposed to determine the time delay D as formula 5.9.

$$R_{y_1y_2}(\bar{\tau}) = E[y_1(t)y_2(t-\bar{\tau})] = \frac{1}{T-\bar{\tau}}\int_{\bar{\tau}}^{T} y_1(t)y_2(t-\bar{\tau})dt \tag{5.9}$$

where E denotes expectation，T is observation interval. The peak of cross correlation function provides an estimate of delay. GCC is aimed to improve the accuracy of the delay estimate $\hat{D}$ where $y_1(t)$ and $y_2(t)$ are filtered. Therefore, the generalized cross correlation function based on the phase transform (PHAT) between $y_1(t)$ and $y_2(t)$ is

$$R_{y1y2}^{(g)}(\bar{\tau}) = \int_{-\infty}^{\infty} \varphi_g(f) G_{y1y2}(f) e^{j2\pi f\bar{\tau}} df \tag{5.10}$$

$$\varphi_g(f) = \frac{1}{\left|G_{y1y2}(f)\right|} \tag{5.11}$$

Ideally, the PHAT weighting function delivers an ideal GCC:

$$R_{y1y2}^{(g)}(\bar{\tau}) = \delta(t-D) \tag{5.12}$$

$$\hat{D} = \underset{d}{^{argmax}}(R_{y1y2}^{(g)}(\bar{\tau})) \tag{5.13}$$

5.3.3 Algorithm of controller design

Step 1: Initialize time-delay estimate $\hat{\tau}$, plant model state estimate $\hat{x}$, reference signal *r* and MPC controller state *xmpc*.

Step 2: Obtain a plant state measurement (i.e., the sensed output states of the plant $x(t-\tau)$), which could be hacked by attackers.

Step 3: Compute the current state estimate, $\hat{x}(t)$, according to the plant state space model. The discrete equation can be approximated as:

$$\dot{\hat{x}}(k+1) = A\hat{x}(k) + Bu(k) + F\Delta P_{load}(k)$$

Step 4: Use GCC algorithm to compute the time-delay estimate $\hat{\tau}$ by comparing historical data $\hat{x}(t)$ and $x(t-\tau)$. In order to reduce the computation complexity, an observation interval *T* is utilized to compute the cross-correlation function.

Step 5: Modify MPC controller state model with time-delay estimate $\hat{\tau}$ obtained in step 3. And then compute the new MPC controller state *xmpc*.

Step 6: Compute the control signal $u(t)$ in the MPC controller. As new MPC controller state *xmpc* and the input of MPC controller $e(t) = r(t) - x(t-\tau)$ are known, u can be set by MPC algorithm.

Step 7: To prevent runaway and dead-zone situations, bound time-delay estimate by $\tau_{\max}$ and the control signal by $\pm u_{\max}$.

Step 8: Repeat step 2-7 in the case of tracking a reference trajectory *r*.

Chapter 6: Case study

6.1 Modified MPC model simulation

To verify the effectiveness and advantages of modified MPC control strategy, three cases are designed to analyze the microgrid frequency response:

1). A constant time-delay attack is applied into system with 0.1 pu load increase

2). A time-varying delay attack is applied into system with 0.1 pu load increase

3). A time-varying delay attack is applied into system with changing load disturbance

By simulating those three cases, the time window of GCC is set as 2s and the MPC controller will be implemented in MATLAB.

6.1.1 Case 1: constant time-delay attack

In this case, the system works in islanded mode. Then, load power increases 0.1 pu since t=2s, and a 0.2s constant time-delay attack is applied into communication channel. Taking the modified MPC control method, online delay estimation and the system frequency control performance is shown Figure 6.1 and Figure 6.2, respectively.

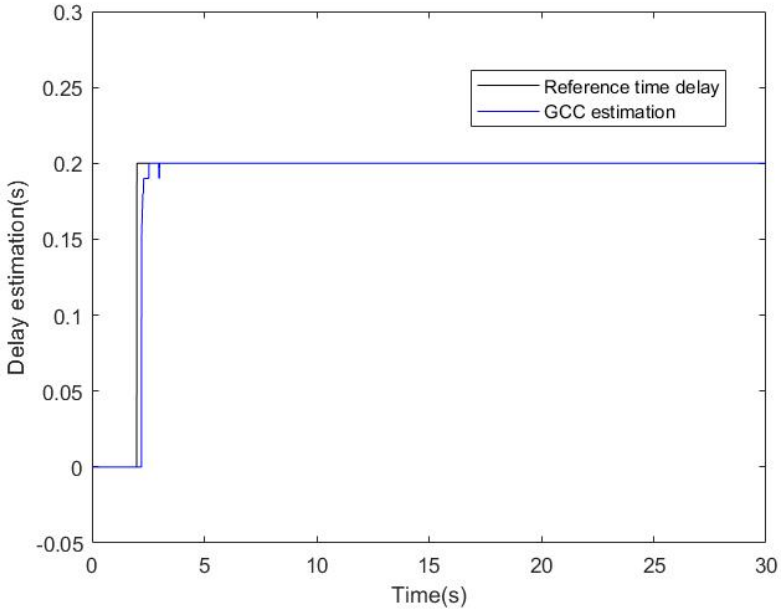

Figure 37.1 GCC delay estimation in case1

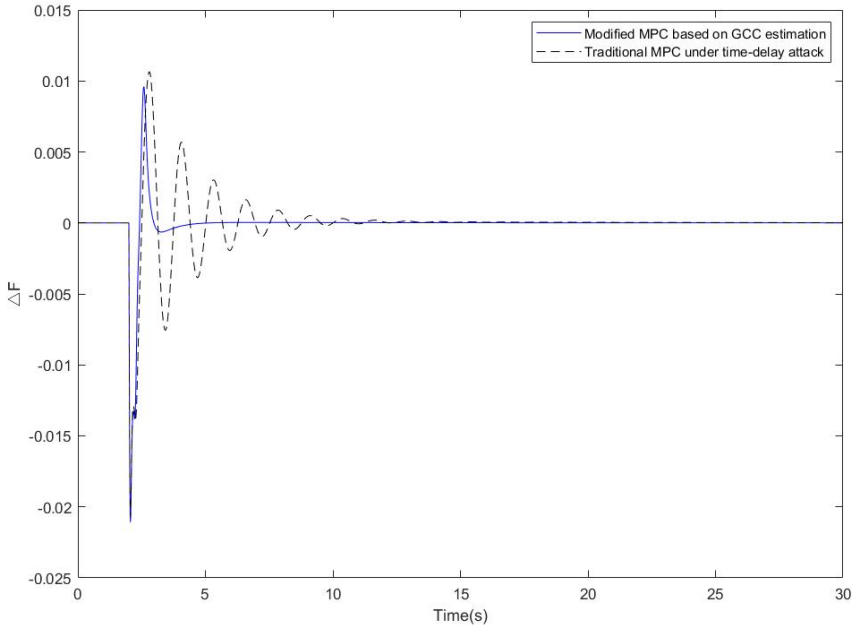

Figure 38.2 Frequency response following a step load disturbance of 0.1 pu

From Figure 6.1, we can see that GCC estimation method can detect and track the time-delay attack with approximately 0.5s error, which is quite appealing. Thus, after acquiring accurate delay time, the state estimation in MPC can work as condition. It can be observed in Figure 6.2 that modified MPC algorithm based on GCC estimation can make system frequency

stable with less than 3s adjustment time and 0.02 pu overshoot. On the other side, traditional MPC needs 10s to realize secondary frequency control and has worse control performance.

6.1.2 Case 2: time-varying delay attack

Case 2 are almost similar to Case 1, except for the delay attack signal. In this case, time delay is 0.2s from t=2s to t=3s and it changes to 0.4s after t=3s. Figure 6.3 shows the frequency output of system and time-varying delay estimation. Load power increases 0.1 pu since t=2s, causing a frequency decrease by the function as droop control at first. Therefore, MPC as a secondary frequency control scheme is designed to balance the power generation and load demand to control the frequency.

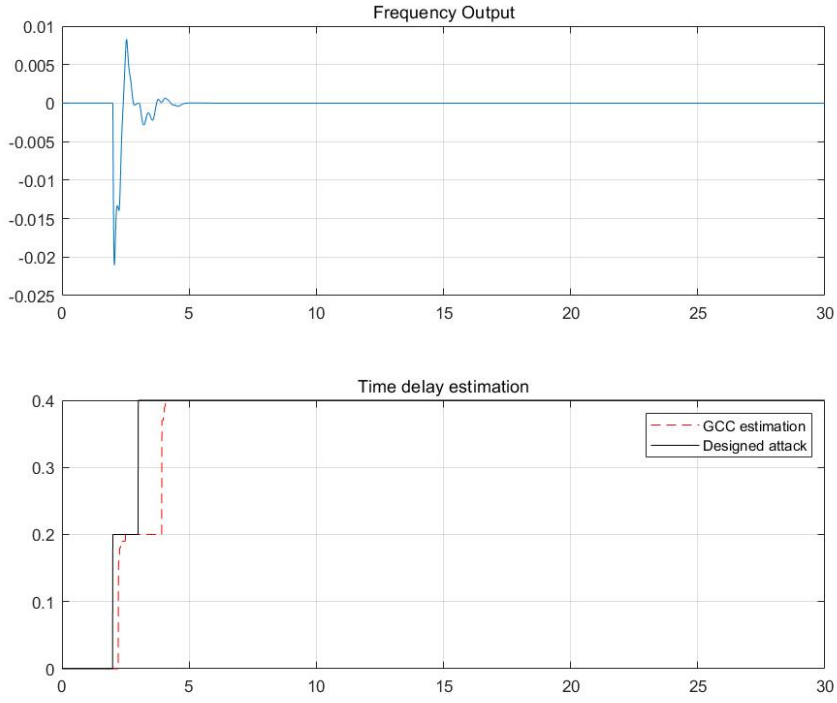

Figure 39.3 (a) Frequency output of microgrid system in case 2 (b) time-varying delay estimation

It shows that modified MPC algorithm based on GCC estimation can also obtain satisfying performance under time-varying delay. The frequency of system maintains stable after t=5s

and the overshoot is about 0.02 pu. Under this circumstance, even when the time-delay attack changes with a short interval, the proposed method will compensate the frequency deviation as the function of secondary frequency control system.

6.1.3 Case 3: two steps load disturbance

In this case, load disturbance has two steps where it's 0.1 pu from t=2s to t=10s and 0.2 pu after t=10s, which is shown in Figure 6.4. On the other hand, time delay is 0.2s from t=2s to t=10s and it changes to 0.4s after t=10s. Figure 6.5 and Figure 6.6 show time-varying delay estimation and the frequency response of microgrid system, respectively.

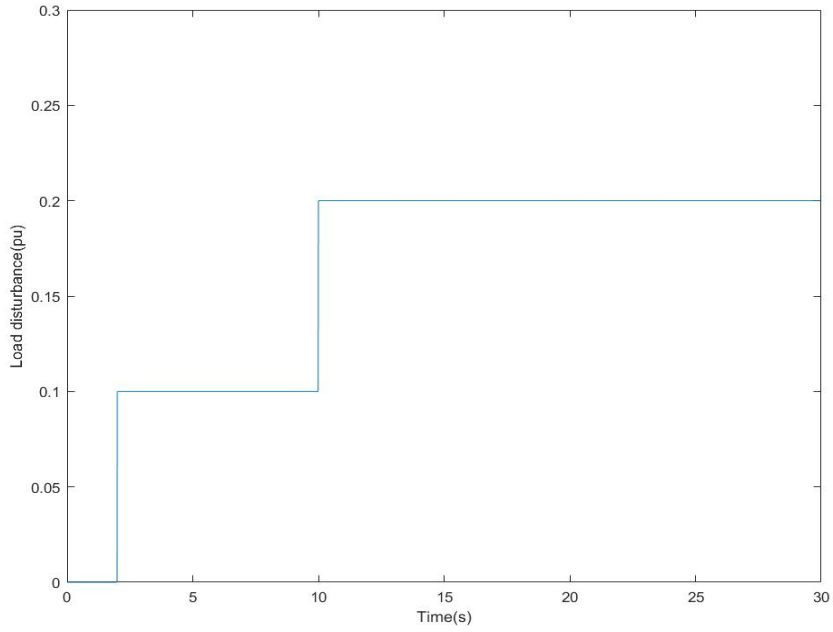

Figure 40.4 Two steps load disturbance

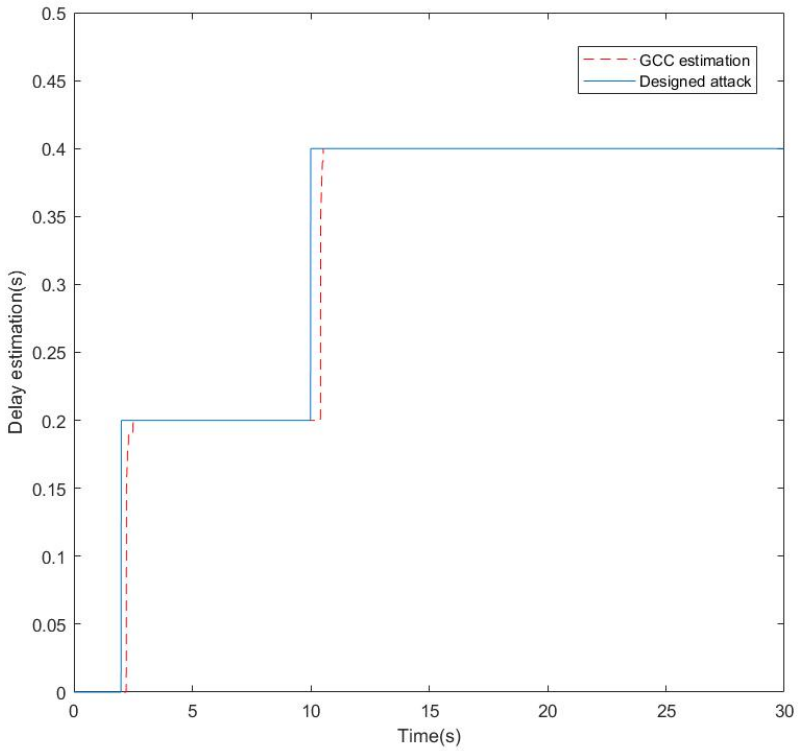

Figure 41.5 GCC time delay estimation in case 3

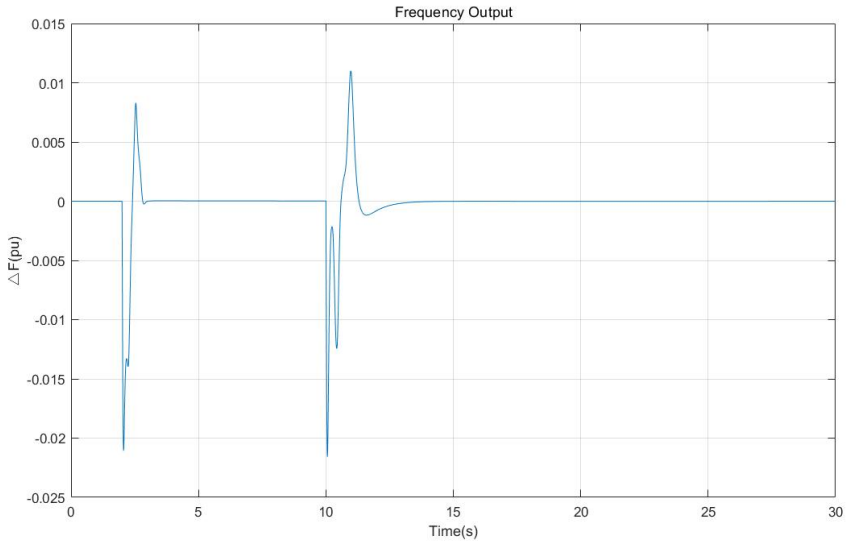

Figure 42.6 Frequency response in case 3

From Figure 6.5, GCC estimation can track the original time-delay attack correctly with little deviation. From Figure 6.6, we can see that there are two peaks when τ=0.4s, which would be higher than τ=0.2s. In other words, due to the longer delay time, the latter control

process is more severe than the former period. But the result can still verify the effectiveness of modified MPC control method under two steps load disturbance with time-varying delay attack.

6.2 Discussion

After analyzing the results of the three case studies mentioned above, we can gain the following conclusions:

(1) The proposed modified MPC can handle the risk under constant and time-varying delay, managing short-term load disturbance successfully. Time-delay attack can be detected and time-delay tracked by GCC method.

(2) The modified MPC control strategy can keep the frequency of microgrid stable under different load disturbance and various time delay attack (e.g. one changing fast in a short time) in real-time operation.

(3) The key part of Modified MPC control strategy is the GCC time-delay estimator, which directly influence the model description and performance of dynamic system. The maximum of time delay attack that the proposed method can handle is 0.8s, otherwise the frequency deviation will be divergent.

(4) After some experiments, various observation time of GCC, during which cross correlation function is calculated to obtain time delay estimation, may lead to different estimation results.

Chapter 7: Conclusion and future work

7.1 Conclusion

In this thesis, the hierarchical structure of microgrid control systems is studied by introducing primary, secondary, and tertiary controls to address different significances and time scales among microgrid control demand. We focus on the secondary frequency control system. The studied islanded microgrid consists of DEG, PV panel, WTG, FC system, BESS, and FESS. All above components can be described by transfer function as a first-order model. Then, the conventional PI controller is simulated in Simulink to compensate frequency deviation under load disturbance. However, in case of any change in the operating conditions, the PI controllers cannot provide the assigned desirable performance. MPC is applied as a suitable intelligent method to compare with the PI controller. The results simulated in MATLAB show that the MPC controller has less overshoot and faster response speed, reaching the desirable operation demand. Three case studies in Chapter 3 verify the robustness of the MPC controller under dynamic change.

On the other side, we find that BESS and FESS have the ability to supply insufficient generation subsystems within a short time. When BESS and FESS lose their responsible ability, there is trifling difference between the PI control method and the MPC control method. The status feedback attack to the MPC controller is considered. The wrong status feedback of BESS and FESS systems may lead to unrecoverable instability to the microgrid system. Therefore, an online switching method based on RMSE is proposed to identify the original status feedback

of BESS and FESS. A simple case study is designed to analyze the detriment caused by the status feedback attack and to verify the effectiveness of the proposed method to protect the control system from such an attack.

Regarding the cyber-security of the microgrid system, time delay attack occurred in the communication channel by an adversary is mainly discussed. To prevent the secondary frequency control of the microgrid system from time-delay attacks, a modified MPC method based on GCC estimation is proposed. During the online operation, time delay can be estimated by GCC and then the state estimation in MPC controller can update. According to the updated plant model, the MPC controller could adjust its control signal to eliminate the fluctuation caused by unknown delay attacks. Finally, the proposed modified MPC can detect and track both constant and time-varying delays, keeping the frequency of the system successfully stable.

7.2 Future work

In this section, recommendations for future work are listed.

1. Various observation time of GCC, during which cross correlation function is calculated to obtain time delay estimation, may lead to different estimation results. In this thesis, the observation time of GCC is set as 2s. Besides, the maximum of time delay attack under proposed method is 0.8s. In the future, some adjustment should be made in improving the accuracy of GCC estimation.
2. In this thesis, only the LTI system in state feedback was discussed, though the method is general in essence. In the future research, the method will be verified that it also works for a class of nonlinear systems.
3. In this thesis, the simulation model assumes that the wind speed and solar radiation

remain a smooth curve. However, in the real microgrid system, we need to consider the disturbance of wind speed and solar radiation. For my future work, more case studies considering fluctuations of wind speed and solar radiation will be designed.

REFERENCES

[1] International Energy Agency. World Energy Outlook. https://www.iea.org/weo2018/ .

[2] N. Hatziargyriou, H. Asano, R. Iravani, and C. Marnay, "Microgrids," IEEE Power Energy Mag., vol. 5, no. 4, pp. 78–94, Jul./Aug. 2007.

[3] T. Ustun, C. Ozansoy, A. Zayegh. Recent developments in microgrids and example cases around the world. A review. Renew Sustain Energy Rev2011;15(8):4030–41.

[4] K. Alanne, A. Saari. Distributed energy generation and sustainable development. Renew Sustain Energy Rev 2006;10(6):539–58.

[5] C.M. Closon, M.H. Nehrir, Algorithms for distributed decision-making for multi-agent microgrid power management. In Proceedings of the IEEE Power and Energy Society General Meeting, Detroit, MI, USA,24–29 July 2011; pp. 1–8.

[6] M. E. Khodayar, M. Barati, and M. Shahidehpour, "Integration of high reliability distribution system in microgrid operation," IEEE Trans.Smart Grid, vol. 3, no. 4, pp. 1997–2006, Dec. 2012.

[7] R. Lasseter and P. Piagi, "Microgrid: A conceptual solution," in Proc. IEEE Annu. Power Electron Specialists Conf., Jun. 2004, pp. 4285–4290.

[8] (Mar.2019). Industrial control systems are still vulnerable to malicious cyberattacks [online]. Available: https://www.technologyreview.com/s/612829/industrial-control-systems-are-still-vulnerable-to-malicious-cyberattacks/

[9] (Mar.2019). Cybersecurity for Critical Infrastructure Protection. [Online]. Available: https://www.gao.gov/new.items/d04321.pdf

[10] R. McMillan, "Siemens: Stuxnet worm hit industrial systems," COMPUTER World, Sept. 2010.

[11] R.M. Lee, M.J. Assante, T. Conway, Analysis of the Cyber Attack on the Ukrainian Power Grid; Electricity Information Sharing and Analysis Center (E-ISAC): Washington, DC, USA, 18 March 2016.

[12] K. Manandhar, X. Cao, F. Hu and Y. Liu, "Detection of Faults and Attacks Including False Data Injection Attack in Smart Grid Using Kalman Filter," in IEEE Transactions on Control of Network Systems, vol. 1, no. 4, pp. 370-379, Dec. 2014.

[13] Y. Liu, P. Ning, and M. K. Reiter, “False data injection attacks against state estimation in electric power grids,” ACM Trans. Inf. Syst. Security, vol. 14, no. 1, p. 13, 2011.

[14] I. Kamwa, R. Grondin, and Y. Hebert, “Wide-area measurement based stabilizing control of large power systems—A decentralized/hierarchical approach,” IEEE Trans. Power Syst., vol. 16, no. 1, pp. 136–153, Feb. 2001.

[15] H. X. Wu, K. S. Tsakalis, and G. T. Heydt, “Evaluation of time delay effects to wide-area power system stabilizer design,” IEEE Trans. Power Syst., vol. 19, no. 4, pp. 1935–1941, Nov. 2004.

[16] Q. Jiang, Z. Zou, and Y. Cao, “Wide-area TCSC controller design in consideration of feedback signals’ time delays,” in Proc. IEEE Power Eng. Soc.Gen.Meeting, vol. 2. San Francisco,CA, USA, 2005, pp. 1676–1680.

[17] Y.L. Huang, A.A. Cárdenas, S. Amin, Z.S. Lin, H.Y. Tsai, S. Sastry, Understanding the physical and economic consequences of attacks on control systems, International Journal of Critical Infrastructure Protection, Volume 2, Issue 3, 2009, Pages 73-83, ISSN 1874-5482.

[18] D. Dotta, A. S. e Silva, and I. C. Decker, “Wide-area measurementsbased two-level control design considering signal transmission delay,” IEEE Trans. Power Syst., vol. 24, no. 1, pp. 208–216, Feb. 2009.

[19] C.-K. Zhang, L. Jiang, Q. H. Wu, Y. He, and M. Wu, “Delay-dependent robust load frequency control for time delay power systems,” IEEE Trans. Power Syst., vol. 28, no. 3, pp. 2192–2201, Aug. 2013.

[20] A. Sargolzaei, K. K. Yen and M. N. Abdelghani, "Preventing Time-Delay Switch Attack on Load Frequency Control in Distributed Power Systems," in IEEE Transactions on Smart Grid, vol. 7, no. 2, pp. 1176-1185, March 2016.

[21] L. Jiang, W. Yao, Q. H. Wu, J. Y. Wen and S. J. Cheng, "Delay-Dependent Stability for Load Frequency Control With Constant and Time-Varying Delays," in IEEE Transactions on Power Systems, vol. 27, no. 2, pp. 932-941, May 2012.

[22] D. E. Olivares et al., "Trends in Microgrid Control," in IEEE Transactions on Smart Grid, vol. 5, no. 4, pp. 1905-1919, July 2014.

[23] J. M. Guerrero, J. C. Vasquez, J. Matas, L. G. de Vicuña, and M. Castilla, “Hierarchical control of droop-controlled AC and DC microgrids—A general approach towards standardization,” IEEE Trans. Ind. Electron., vol. 58, no. 1, pp. 158–172, Jan. 2011.

[24] J. A. P. Lopes, C. L. Moreira, and A. G. Madureira, “Defining control strategies formicrogrids islanded operation,” IEEE Trans. Power Syst., vol. 21, pp. 916–924, May 2006.

[25] A. Bidram and A. Davoudi, "Hierarchical Structure of Microgrids Control System," in IEEE Transactions on Smart Grid, vol. 3, no. 4, pp. 1963-1976, Dec. 2012.

[26] H. Karimi, E. J. Davison, and R. Iravani, “Multivariable servomechanism controller for autonomous operation of a distributed generation unit: Design and performance evaluation,” IEEE Trans. Power Syst., vol. 25, no. 2, pp. 853–865, May 2010.

[27] B. Bahrani, M. Saeedifard, A. Karimi, and A. Rufer, “A multivariable design methodology for voltage control of a single-DG-unit microgrid,” IEEE Trans. Ind. Electron., vol. 9, no. 2, pp. 589–599, May 2013.

[28] T. L. Vandoorn, J. D. M. De Kooning, B. Meersman, J. M. Guerrero, and L. Vandevelde, “Voltage-based control of a smart transformer in a microgrid,” IEEE Trans. Ind. Electron., vol. 60, no. 4, pp. 1291–1305, Apr. 2013.

[29] T. Iwade, S. Komiyama, and Y. Tanimura, “A novel small-scale UPS using a parallel redundant operation system,” in Proc. Int. Telecommunications Energy Conf., 2003, pp. 480–483.

[30] J. A. P. Lopes, C. L. Moreira, and A. G. Madureira, “Defining control strategies formicrogrids islanded operation,” IEEE Trans. Power Syst., vol. 21, no. 2, pp. 916–924, May 2006.

[31] Y. J. Cheng and E. K. K. Sng, “A novel communication strategy for decentralized control of paralleled multi-inverter systems,” IEEE Trans. Power Electron., vol. 21, pp. 148–156, Jan. 2006.

[32] F. Katiraei, M. R. Iravani, and P. W. Lehn, “Micro-grid autonomous operation during and subsequent to islanding process,” IEEE Trans. Power Del., vol. 20, no. 1, pp. 248–257, Jan. 2005.

[33] H. Bevrani, Robust Power System Frequency Control. New York: Springer, 2009.

[34] S. Obara, “Analysis of a fuel cell micro-grid with a small-scale wind turbine generator,” Int. J. Hydrogen Energy, vol. 32, pp. 323–336, Mar.2007.

[35] Bidram, A. Davoudi, F. L. Lewis, and J. M. Guerrero, “Distributed cooperative secondary control of microgrids using feedback linearization,” IEEE Trans. Power Syst., vol. 28, no. 3, pp. 3462–3470, Aug. 2013.

[36] R. Palma-Behnke et al., “A microgrid energy management system based on the rolling horizon strategy,” IEEE Trans. Smart Grid, vol. 4, no. 2, pp. 996–1006, Jun. 2013.

[37] Y. Khayat et al., "Decentralized Optimal Frequency Control in Autonomous Microgrids," in IEEE Transactions on Power Systems. 2018.

[38] J. M. Rey, P. Marti, M. Velasco, J. Miret, and M. Castilla, “Secondary Switched Control with no Communications for Islanded Microgrids,” IEEE Trans. Ind. Electron., pp. 8534–8545, 2017.

[39] R. Han, L. Meng, J. M. Guerrero, and J. C. Vasquez, “Distributed Nonlinear Control with Event-Triggered Communication to Achieve Current-Sharing and Voltage Regulation in DC Microgrids,” *IEEE Trans. Power Electron.*, pp. 1–1, 2017.

[40] W. Gu, G. Lou, W. Tan, and X. Yuan, “A Nonlinear State Estimator-Based Decentralized Secondary Voltage Control Scheme for Autonomous Microgrids,” *IEEE Trans. Power Syst.*, pp. 4794–4804, 2017.

[41] H. Bevrani, F. Habibi, P. Babahajyani, M. Watanabe and Y. Mitani, "Intelligent Frequency Control in an AC Microgrid: Online PSO-Based Fuzzy Tuning Approach," in IEEE Transactions on Smart Grid, vol. 3, no. 4, pp. 1935-1944, Dec. 2012.

[42] J. M. Guerrero, L. Hang, and J. Uceda, “Control of distributed uninterruptible power supply systems,” IEEE Trans. Ind. Electron., vol. 55, pp. 2845–2859, Aug. 2008.

[43] T. Senjyu, T. Nakaji, K. Uezato, and T. Funabashi, “A hybrid power system using alternative energy facilities in isolated island,” IEEE Trans. Energy Convers., vol. 20, no. 2, pp. 406–414, Jun. 2005.

[44] S. Kouro, P. Cortes, R. Vargas, U. Ammann and J. Rodriguez, "Model Predictive Control—A Simple and Powerful Method to Control Power Converters," in IEEE Transactions on Industrial Electronics, vol. 56, no. 6, pp. 1826-1838, June 2009.

[45] M. B. Shadmand, R. S. Balog and H. Abu-Rub, "Model Predictive Control of PV Sources in a Smart DC Distribution System: Maximum Power Point Tracking and Droop Control," in IEEE Transactions on Energy Conversion, vol. 29, no. 4, pp. 913-921, Dec. 2014.

[46] G. Grimm, M. J. Messina, S. E. Tuna and A. R. Teel, "Nominally Robust Model Predictive Control With State Constraints," in IEEE Transactions on Automatic Control, vol. 52, no. 10, pp. 1856-1870, Oct. 2007.

[47] O. A. Beg, T. T. Johnson and A. Davoudi, "Detection of False-Data Injection Attacks in Cyber-Physical DC Microgrids," in IEEE Transactions on Industrial Informatics, vol. 13, no. 5, pp. 2693-2703, Oct. 2017.

[48] H. Zhang, W. Meng, J. Qi, X. Wang and W. X. Zheng, "Distributed Load Sharing Under False Data Injection Attack in an Inverter-Based Microgrid," in IEEE Transactions on Industrial Electronics, vol. 66, no. 2, pp. 1543-1551, Feb. 2019.

[49] X. Liu, M. Shahidehpour, Y. Cao, L. Wu, W. Wei and X. Liu, "Microgrid Risk Analysis Considering the Impact of Cyber Attacks on Solar PV and ESS Control Systems," in *IEEE Transactions on Smart Grid*, vol. 8, no. 3, pp. 1330-1339, May 2017.

[50] A. Sargolzaei, K. Yen and M. Abdelghani, "Delayed inputs attack on load frequency control in smart grid," *ISGT 2014*, Washington, DC, 2014, pp. 1-5.

[51] C. Knapp and G. Carter, "The generalized correlation method for estimation of time delay," in IEEE Transactions on Acoustics, Speech, and Signal Processing, vol. 24, no. 4, pp. 320-327, August 1976.

[52] M. Azaria and D. Hertz, "Time delay estimation by generalized cross correlation methods," in IEEE Transactions on Acoustics, Speech, and Signal Processing, vol. 32, no. 2, pp. 280-285, April 1984.